

R-modes and neutron star recycling scenario

A. I. Chugunov^{1, *}, M. E. Gusakov¹, E. M. Kantor¹

¹*Ioffe Institute, St Petersburg, Russia*

Accepted 2017 xxxx. Received 2017 xxxx; in original form 2016 xxxx

ABSTRACT

To put new constraints on the r-mode instability window, we analyse the formation of millisecond pulsars (MSPs) within the recycling scenario, making use of three sets of observations: (a) X-ray observations of neutron stars (NSs) in low-mass X-ray binaries; (b) timing of millisecond pulsars; and (c) X-ray and UV observations of MSPs. As shown in previous works, r-mode dissipation by shear viscosity is not sufficient to explain observational set (a), and enhanced r-mode dissipation at the red-shifted internal temperatures $T^\infty \sim 10^8$ K is required to stabilize the observed NSs. Here, we argue that models with enhanced bulk viscosity can hardly lead to a self-consistent explanation of observational set (a) due to strong neutrino emission, which is typical for these models (unrealistically powerful energy source is required to keep NSs at the observed temperatures). We also demonstrate that the observational set (b), combined with the theory of internal heating and NS cooling, provides evidence of enhanced r-mode dissipation at low temperatures, $T^\infty \sim 2 \times 10^7$ K. Observational set (c) allows us to set an upper limit on the internal temperatures of MSPs, $T^\infty < 2 \times 10^7$ K (assuming a canonical NS with the accreted crust). Recycling scenario can produce MSPs at these temperatures only if r-mode instability is suppressed in the whole MSP spin frequency range ($\nu \lesssim 750$ Hz) at temperatures $2 \times 10^7 \lesssim T^\infty \lesssim 3 \times 10^7$ K, providing thus a new constraint on the r-mode instability window. These observational constraints are analysed in more details in application to the resonance uplift scenario of [Gusakov et al. \(2014b,a\)](#).

1 INTRODUCTION

According to the generally accepted recycling scenario ([Bisnovatyi-Kogan & Komberg 1976](#); [Alpar et al. 1982](#)), millisecond pulsars (MSPs) are descendants of neutron stars (NSs), which were spun up by accretion from Roche-lobe filling companion stars in low-mass X-ray binaries (LMXBs). This scenario has been extensively studied in the literature with the main emphasis on the NS spin frequency, evolution of the companion star, and parameters of the binary system (e.g., [Tauris 2012](#); [Chen et al. 2013](#) and references therein). NS temperature has not been typically considered as an important parameter for NS recycling, and is not even mentioned in most of the papers in the field. However, NS temperature is crucial for the instability of r-modes (similar to Rossby waves controlled by the Coriolis force) driven by Chandrasekhar-Friedman-Schutz (CFS; [Chandrasekhar 1970](#); [Friedman & Schutz 1978a,b](#)) mechanism due to emission of gravitational waves ([Andersson 1998](#); [Friedman & Morsink 1998](#)). Namely, if a rapidly rotating NS is hot enough, it becomes unstable with respect to excitation of r-modes (see, e.g., [Lindblom, Owen, & Morsink 1998](#); the corresponding region of NS temperatures and spin frequencies is often referred to as ‘the instability window’). This instability is known to modify the NS evolution in LMXBs dramatically (see section 2.1 and, e.g., [Levin 1999](#); [Bondarescu, Teukolsky, & Wasserman 2007](#);

[Gusakov, Chugunov, & Kantor 2014a](#)). In particular, it can limit rotation frequencies of NSs ([Bildsten 1998](#); [Andersson, Kokkotas, & Stergioulas 1999b](#)). Furthermore, we ([Chugunov, Gusakov, & Kantor 2014](#)) argued that the r-mode instability can lead to additional channel of NS recycling: formation of a new class of NSs — HOFNARs (from HOt and Fast Non-Accreting Rotators) — in addition to MSPs. Thus, accurate account for the r-mode instability should be important for the recycling scenario; conversely, verification of the recycling scenario can put stringent constraints on the r-mode instability and, therefore, on the properties of superdense matter.

In this paper we analyse constraints on the r-mode instability within the recycling scenario. We base our analysis on the following observations:

- (a) X-ray observations of transiently accreting NSs in LMXBs (section 2.2);
- (b) Timing of MSPs (section 2.3);
- (c) X-ray and UV observations of MSPs (section 2.4).

We do not take into consideration observational data on binary system parameters (orbital period, eccentricity etc.), because they seem to be determined by the evolution of binary system (e.g., [Chen et al. 2013](#)) and not affected directly by the r-mode instability.

The set of observations (a) allows one to estimate the

arXiv:1610.06380v2 [astro-ph.HE] 22 Mar 2017

effective surface temperatures (in the quiescent state, see, e.g., [Heinke et al. 2007, 2009](#)) and spin frequencies (e.g., [Watts et al. 2008](#)) for a number of accreting NSs. It has been shown to be a crucial test of the r-mode instability theory ([Ho, Andersson, & Haskell 2011](#); [Haskell, Degenaar, & Ho 2012](#)). In particular, those references have demonstrated that the ‘minimal’ model of r-mode instability window, suggested by [Lindblom et al. \(1998\)](#) (NS has a nucleonic core, r-mode damping is associated with shear and bulk viscosities, see section 2.1), should be supplemented by additional damping mechanism at redshifted internal temperatures $T^\infty \sim (3 \times 10^7 - 10^8) \text{ K}^1$ (alternatively, saturation amplitude for r-modes should be extremely small, the so called ‘tiny r-mode amplitude scenario’, see section 3 and, e.g., [Mahmoodifar & Strohmayer 2013](#)). A number of papers are devoted to the identification of the required damping mechanism (see the recent review by [Haskell 2015](#)). In particular, [Gusakov et al. \(2014b,a\)](#) argues that finite temperature effects in superfluid NS cores can lead to resonance mode coupling and suppression of the r-mode instability at certain stellar temperatures. As a result, the instability window is splitted up by ‘stability peaks’ in the vicinity of these temperatures. [Gusakov et al. \(2014b,a\)](#) discuss evolution of NSs in LMXBs within this model and suggest a ‘resonance uplift scenario’, which allows them to explain the observational set (a). Other ideas about the required additional damping include enhanced mutual friction (e.g., [Haskell et al. 2009](#)), crust-core coupling (e.g., [Rieutord 2001](#); [Levin & Ushomirsky 2001](#); [Glampedakis & Andersson 2006a,b](#)), and exotic core composition (e.g., [Jones 2001b](#); [Lindblom & Owen 2002](#); [Nayyar & Owen 2006](#); [Alford & Schwenzer 2014b](#)). Concerning the observational set (a) we point out that any successful theory should not only stabilize the observed NSs in LMXBs, but also explain their temperatures.

MSP timing [set of observations (b); see section 2.3] has also been used to constrain the r-mode instability. [Reisenegger & Bonačić \(2003b\)](#) discuss formation of MSPs assuming bulk viscosity driven suppression of r-mode instability. They predict that spin down of the fastest MSPs can be affected by r-modes. Furthermore, these NSs should have internal temperatures $T^\infty \sim 2 \times 10^7 \text{ K}$, being the sources of thermal X-rays. [Gusakov et al. \(2014a\)](#) analyse formation of recycled NSs within the resonance uplift scenario and concluded that it does not contradict the idea that MSPs are descendants of NSs in LMXBs. They also predict that the most rapidly rotating MSPs should be rather hot (with internal temperatures $T^\infty \sim 10^7 \text{ K}$) due to r-mode heating. [Owen \(2010\)](#); [Alford & Schwenzer \(2015\)](#) argue that the minimal instability model requires extremely small r-mode saturation amplitudes to match the observed pulsars’ spin-down. [Alford & Schwenzer \(2014b\)](#) discuss MSP formation and conclude that compact stars with the cores composed of ‘ungapped interacting quark matter’ are consistent with observations of LMXBs and MSPs (see a critique of this statement in section 4). They also confirm

that additional damping is required to describe MSPs by the models with nucleonic core composition. In this paper (section 2.3) we present an independent argument in favour of enhanced r-mode damping at low temperatures, based on the MSP internal heating mechanisms: superfluid vortex creep ([Alpar et al. 1984](#)), rotochemical heating ([Reisenegger 1995](#)), and rotation-induced deep crustal heating ([Gusakov, Kantor, & Reisenegger 2015](#)).

The X-ray and *UV* observations [set (c), section 2.4] attract less attention in the r-mode literature, because the data for most of the observed MSPs do not require thermal emission from the whole surface (but only from hot spots; see, e.g., [Zavlin 2007](#); [Bogdanov et al. 2011b](#)) and the surface temperature is measured only for PSR J0437-4715 by [Durant et al. \(2012\)](#) and for PSR J2124-3358 by [Rangelov et al. \(2017\)](#). For other MSPs the surface temperature is thought of as ‘generally unknown’ ([Alford & Schwenzer 2014b](#)) or not too high [namely, [Reisenegger & Bonačić 2003b](#) argue that MSP temperatures are ‘below the upper limits from observations of MSPs with the ROSAT (Roentgen Satellite) X-ray telescope’ and [Gusakov et al. 2014a](#); [Chugunov et al. 2014](#) assume that redshifted surface temperature of MSPs can be bounded by $T_{\text{eff}}^\infty \lesssim 10^6 \text{ K}$]. Upper limits for internal temperature of several MSPs are also shown in Fig. 1 of [Andersson, Jones, & Kokkotas \(2002\)](#). In this paper we argue that X-ray and *UV* observations allow one to put an upper limit on the redshifted surface temperature of MSPs, $T_{\text{eff}}^\infty < T_{\text{eff, max}}^\infty$, and argue that $T_{\text{eff, max}}^\infty = 6 \times 10^5 \text{ K}$ can be chosen as a fiducial value, applicable to all MSPs (otherwise thermal emission from the whole surface should be observed, see section 2.4). It corresponds to an upper limit on the internal temperatures of MSPs: $T^\infty < T_{\text{max}}^\infty = 2 \times 10^7 \text{ K}$ (here and below, to estimate internal temperatures of NSs, we consider a canonical NS with the mass $M = 1.4M_\odot$ and $R = 10 \text{ km}$, and use the accreted envelope model from [Potekhin et al. 1997](#)). This constraint is crucial for r-mode instability models, because any successful model should not only stabilize NSs at these temperatures (in the opposite case r-mode instability heats MSPs up to higher temperatures), but also explain how they came into this temperature region.

In sections 3–6 we apply the observations (a–c) to constrain the r-mode instability parameters. Namely, in section 3 we improve constraints on the tiny r-mode amplitude scenario. In section 4 we analyse models based on an enhanced bulk viscosity, in particular, the ungapped interacting quark matter model, suggested by [Alford & Schwenzer \(2014b\)](#), and conclude that it cannot explain temperatures of the hottest NSs in LMXBs. In section 5 we analyse the resonance uplift scenario. We demonstrate that low-temperature stability peaks at $T^\infty \lesssim 2 \times 10^7 \text{ K}$ are required by observations, and they should be broad. These results are extended to a quite general class of r-mode instability models (a set of humps of enhanced stability located at certain temperatures) in section 6. We conclude in section 7.

During the final stage of the preparation of this manuscript we became aware of the work by [Schwenzer et al. \(2017\)](#), who also use X-ray observations to constrain MSP temperatures and derive upper bounds on the r-mode amplitudes for these sources. The results of our section 3 qualitatively agree with those of [Schwenzer et al. \(2017\)](#).

¹ Following [Gusakov et al. \(2014b,a\)](#), we characterize thermal states of NSs by the redshifted temperature T^∞ , rather than by the local temperature T , because it is T^∞ , which is constant throughout the star.

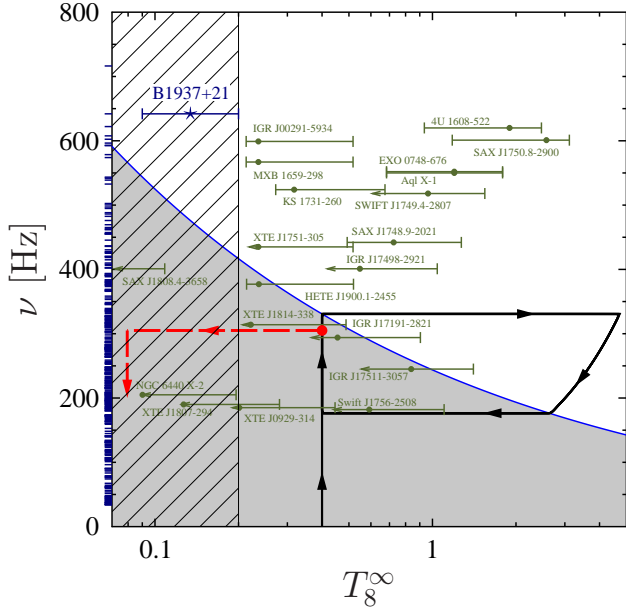


Figure 1. Minimal r-mode instability model for a canonical NS. The stability region is shaded in grey; in the white region the r-mode is unstable. Hatched region corresponds to the observational limit (8) on the MSP temperature. Temperatures and frequencies of NSs observed in LMXBs are shown by filled circles, error bars show uncertainties due to NS envelope composition (section 2.2). The pulsar B1937+21 is shown by star; its low-temperature error bar is set by the rotation-induced deep crustal heating (see section 2.3), the upper error bar is set by the fiducial limit (8) on the MSP temperature. Ticks on the left side of ν axis show measured MSP frequencies. Typical evolution track for a NS in LMXB is shown by a thick black line, and a large filled circle marks the end of LMXB stage. The dashed line demonstrates evolution track of a star in the MSP stage.

The preliminary results of this work were presented by one of us (AIC) at two conferences: (i) ‘The Modern Physics of Compact Stars and Relativistic Gravity 2015’ (September 30 – October 3; Yerevan, Armenia, 2015); and (ii) ‘The International Workshop on Quark Phase Transition in Compact Objects and Multimessenger Astronomy: Neutrino Signals, Supernovae and Gamma-Ray Bursts’ (October 7 – October 14; Nizhnij Arkhyz & Terskol, Russia, 2015).

2 MINIMAL R-MODE INSTABILITY MODEL VS OBSERVATIONS: ADDITIONAL DISSIPATION IS REQUIRED

In this section we describe the minimal r-mode instability model and confront it with each of the three sets of observations (a)–(c) from Section 1.

2.1 Minimal r-mode instability model

In the absence of damping the gravitational radiation reaction force leads to exponential growth of the r-mode amplitude on a timescale (see, e.g., Lindblom, Owen, & Morsink 1998; Friedman, Lindblom, & Lockitch 2016)

$$\tau_{\text{GR}} \approx -3000 \text{ s } M_{1.4}^{-1} R_{10}^{-4} \nu_{500}^{-6}. \quad (1)$$

Here NS mass M and radius R are normalized to the mass and radius of the canonical NS: $M_{1.4} = M/(1.4 M_{\odot})$, $R_{10} = R/(10 \text{ km})$, and $\nu_{500} = \nu/(500 \text{ Hz})$. Here $\nu = \Omega/2\pi$ is the NS spin rate. The numerical coefficients in equation (1) and other equations in this section correspond to a Newtonian star with polytropic equation of state ($P \propto \rho^2$).

The minimal r-mode instability model suggested by Lindblom et al. (1998) includes shear and bulk viscosities as damping agents and assumes nucleonic equation of state. The shear viscosity damping time can be estimated as²

$$\tau_{\text{s}} = 2.2 \times 10^5 \text{ s } R_{10}^5 M_{1.4}^{-1} (T_8^{\infty})^2, \quad (2)$$

where $T_8^{\infty} = T^{\infty}/10^8 \text{ K}$. The bulk viscosity damping time was calculated by Lindblom, Mendell, & Owen (1999):

$$\tau_{\text{b}} = 2.8 \times 10^{18} \text{ s } M_{1.4} \nu_{500}^{-2} R_{10}^{-3} (T_8^{\infty})^{-6}. \quad (3)$$

The total damping time is $\tau_{\text{d}} = 1/(\tau_{\text{s}}^{-1} + \tau_{\text{b}}^{-1})$, however, the effect of bulk viscosity is negligible for temperatures of MSPs and NSs in LMXBs. The r-mode is stable if $\tau_{\text{GR}}^{-1} + \tau_{\text{d}}^{-1} > 0$ (grey region in Fig. 1) and unstable in the opposite case $\tau_{\text{GR}}^{-1} + \tau_{\text{d}}^{-1} < 0$ (white region in Fig. 1). In the unstable region the r-mode amplitude is growing until it reaches saturation, where the nonlinear effects become important (see, e.g., Arras et al. 2003; Bondarescu et al. 2007; Bondarescu & Wasserman 2013; Haskell, Glampedakis, & Andersson 2014).

Gravitational waves emitted by r-modes reduce stellar angular momentum J at a rate

$$\dot{J}_{\text{GR}} = \frac{3\tilde{J}MR^2\Omega\alpha^2}{\tau_{\text{GR}}}. \quad (4)$$

The dissipation of r-mode leads to additional heating power (e.g., Alford & Schwenzer 2014a; Gusakov et al. 2014a)

$$W^{\text{r}} = \frac{\tilde{J}MR^2\Omega^2\alpha^2}{\tau_{\text{eff}}}, \quad (5)$$

where $\tau_{\text{eff}} = |\tau_{\text{GR}}|$ for saturated and $\tau_{\text{eff}} = \tau_{\text{d}}$ for unsaturated r-mode, respectively, and $\tilde{J} \approx 0.016$.

General equations that describe evolution of a NS affected by r-mode instability were formulated by Lindblom et al. (1998) (see also Levin 1999; Ho & Lai 2000; Alford & Schwenzer 2014a; Gusakov et al. 2014b) and the typical evolution track is shown by a thick black line in Fig. 1. During the initial phase NS is spinned up by accretion and its temperature $T^{\infty} = T_{\text{eq}}^{\infty}$ is determined by the balance between the cooling [the corresponding emissivity is $L_{\text{cool}}(T^{\infty})$] and deep crustal heating W^{DCH} (Brown, Bildsten, & Rutledge 1998):

$$L_{\text{cool}}(T_{\text{eq}}^{\infty}) = W^{\text{DCH}} = Kc^2 \dot{M}. \quad (6)$$

Here the coefficient $K \sim 10^{-3}$ determines efficiency of deep crustal heating. As shown by Levin (1999), when a NS enters the instability region due to continuous accretion, the

² See a discussion of the electron and nucleon contribution to the shear viscosity in Gusakov et al. (2014a). Note that the shear viscosity employed by Alford & Schwenzer (2014b) differs from that in Gusakov et al. (2014a) because the latter authors assumed that protons are superconducting, while in Alford & Schwenzer (2014b) they were considered normal [see Shternin & Yakovlev (2008) for a detailed analysis of the superconductivity effects on the shear viscosity].

r-mode amplitude starts to grow and its subsequent evolution is very fast (provided that the saturation amplitude is not too small, see appendix B in [Gusakov et al. 2014a](#) for a set of analytical estimates). Eventually, the star rapidly heats up and slows down, leaving the instability region. In the stable region it gradually cools down to the temperature T_{eq}^{∞} , and a new spin up cycle starts again. In principle, during its life a NS in LMXB can complete several such cycles but it is important that the probability to catch it in the instability region is negligible. After Roche-lobe decoupling (see the filled circle in the evolution curve in Fig. 1) a star cools down and an MSP is formed (MSP evolution track is shown by a dashed line). MSP spin frequency is limited by the r-mode instability curve ([Bildsten 1998](#); [Andersson, Kokkotas, & Schutz 1999a](#)).

2.2 X-ray observations of transiently accreting neutron stars in LMXBs

X-ray observations of some of the transiently accreting NSs allow one to measure their surface temperature in the quiescent state (e.g., [Heinke et al. 2007, 2009](#)). The internal temperature can be inferred from the surface temperature, assuming thermally relaxed envelope, with the help of analytical fitting formulas presented in [Potekhin et al. \(1997\)](#). Furthermore, the spin frequency can be measured for accretion- and nuclear-powered MSPs (e.g., [Watts et al. 2008](#)). As a result, both spin frequency and internal temperature are available for a rather large number of objects ([Ho et al. 2011](#); [Haskell et al. 2012](#); [Gusakov et al. 2014a](#)).

In addition, observations of transiently accreting NSs in the active state allow one to estimate average accretion rate and the corresponding heating power associated with nuclear reactions in the accreted crust (e.g., [Heinke et al. 2007, 2009](#)).

In this paper we employ the data for 20 NSs from table I of [Gusakov et al. \(2014a\)](#), where a number of misprints found in the previous works have been corrected (see dots with error bars in Fig. 1, temperature for HETE J1900.1-2455 was updated according to [Degenaar et al. \(2017\)](#), $T_{\text{eff}}^{\infty} = 6.3 \times 10^5$ K). At least 8 NSs among them are predicted to be r-mode unstable within the minimal r-mode instability model. However, a probability to observe even one NS unstable is almost vanishing within the minimal r-mode instability model (see section 2.1). Thus, observations of a large number of NSs, which appear to be unstable, can be treated as evidence of additional (apart from the shear viscosity) damping at the temperatures of these objects, $T^{\infty} \sim 3 \times 10^7 - 10^8$ K, or r-mode saturation at very small saturation amplitude (e.g., [Ho et al. 2011](#); [Haskell et al. 2012](#); [Gusakov et al. 2014a](#); [Mahmoodifar & Strohmayer 2013](#)). Note that this problem can hardly be resolved by enhancing the shear viscosity (e.g., to stabilize 4U 1608–522 one should enhance it by a factor of 1000, and we are unaware of any physically motivated mechanism predicting such a strong enhancement) or by fitting the mass-radius relation [for example, 4U 1608–522 should be stable according to equations (1)–(2) if radius $R \lesssim 5$ km. However, these equations are written for a baryonic equation of state, and thus they are inapplicable for such a small radius, because such equations of state predict larger radii (see, e.g., [Oertel, Hempel, Klöhn, & Typel 2016](#);

[Zdunik, Fortin, & Haensel 2016](#)); observations also favour larger NS radii (e.g., [Özel & Freire 2016](#))].

2.3 Timing of MSPs

Timing of MSPs allows one to measure the spin frequency (see ticks on the left side of ν axis in Fig. 1; only pulsars with $\nu > 33$ Hz are shown in the figure) and the spin-down rate. These data were taken from ATNF Pulsar Catalogue ([Manchester et al. 2005](#), catalogue version 1.55 was applied).³

Within the minimal r-mode instability model MSP spin frequencies should be limited by the r-mode instability. Thus, the origin of the high frequency MSPs (especially those with $\nu \gtrsim 600$ Hz) is unclear in this model, because they should have very low equilibrium temperatures ($T^{\infty} \lesssim 10^7$ K) to be stable during the spin up in the LMXB stage (see Fig. 1). As shown in sections 5.2 and 6, such low temperatures are incompatible with existing accretion and cooling models. Thus, formation of MSPs requires additional damping or use of a tiny saturation amplitude model (see section 3 and, e.g., [Alford & Schwenzer 2014b](#)).

Another constraint on the r-mode instability comes from the internal heating mechanisms – superfluid vortex creep ([Alpar et al. 1984](#)), rotochemical heating ([Reisenegger 1995](#)), and rotation-induced deep crustal heating ([Gusakov et al. 2015](#)) – which can be efficient enough to push PSR B1937+21 (J1939+2134 in J2000 system) into the r-mode instability window (see Fig. 1). To estimate the internal heating power W^i for MSPs we rely on the rotation-induced deep crustal heating mechanism, because it is not affected by the uncertainties in the parameters of baryon superfluidity. Physics of rotation-induced deep crustal heating is rather simple. MSP spin-down (e.g., by magnetodipole losses) results in a gradual compression of stellar matter. Within the recycling scenario paradigm, the crust of MSPs should consist of accreted matter, thus the compression should lead to the same nuclear transformations in the crust as in the case of accreting NSs (i.e., to deep crustal heating). For example, for PSR B1937+21 which has high frequency ($\nu \approx 642$ Hz) and relatively fast spin-down rate ($\dot{\nu} \approx 4.3 \times 10^{-14}$ s⁻²), the rotation-induced deep crustal heating (which is generally proportional to $W^i \propto \nu \dot{\nu}$) gives $W^i \sim (10^{31} - 2 \times 10^{32})$ ergs⁻¹, depending on the equation of state and pulsar mass. To balance this heating power at the lowest possible temperature (in order to get it stable), a powerful cooling process should be active in the core of this source. To get an impression of the possible realistic cooling luminosity, we adopt here a simple phenomenological model, which assumes that the unsuppressed hyperon direct URCA process (see, e.g., [Yakovlev et al. 2001](#)) is active in the central region of the core with the radius R_D , where hyperons are present (see [Kantor, Gusakov, & Chugunov 2016](#) for a

³ <http://www.atnf.csiro.au/research/pulsar/psrcat/expert.html>

detailed motivation). The corresponding luminosity is⁴

$$L_{\text{cool}}^{\text{URCA}} \approx 10^{33} \text{ erg s}^{-1} \left(\frac{T^\infty}{2 \times 10^7 \text{ K}} \right)^6 \left(\frac{R_D}{3 \text{ km}} \right)^3. \quad (7)$$

For $R_D = 3 \text{ km}$ the equilibrium temperature of PSR B1937+21, at which $W^i \approx L_{\text{cool}}^{\text{URCA}}$, can be estimated as $T^\infty \sim (0.9\text{--}1.5) \times 10^7 \text{ K}$. In the absence of direct URCA, the equilibrium temperature becomes larger, so that the source is well inside the instability window (see Fig. 1, where it is shown by the star symbol). Note that some other internal heating mechanisms (see, e.g., [Gonzalez & Reisenegger 2010](#) for a review) can be competitive with the rotation-induced deep crustal heating, further increasing the temperature of PSR B1937+21 and making it even more unstable. However, as explained in section 2.1, r-modes rapidly heat up an unstable star (on a timescale of a century) and spin it down. Thus, observations of PSR B1937+21 contradict the minimal r-mode instability model: To explain this source one should stabilize it by introducing an additional damping mechanism, which prevents r-modes from being unstable.

Summarizing, current state of high-frequency MSPs can be explained within the minimal r-mode instability model only if they are cold enough to be stable. However, this explanation has two problems: (i) MSPs cannot be produced by accretion at such low temperatures; (ii) PSR B1937+21 cannot be in thermal equilibrium inside the stability region (cooling cannot compensate internal heating). As discussed below, both problems can be resolved within the tiny r-mode saturation amplitude scenario (but then the required saturation amplitudes are unfeasible, at least for hadronic equations of state, see section 3) or by additional dissipation of r-modes at $T^\infty \sim 2 \times 10^7 \text{ K}$ (sections 4–6).

2.4 X-ray and UV observations of MSPs

The NS temperature is a crucial parameter for the r-mode instability and hence any observational constraint on the stellar temperature can be very important. A large number of MSPs has been observed in X-rays, however, the thermal emission from them has been either not detected or detected only from pulsars' hot spots (e.g., [Zavlin 2007](#); [Bogdanov et al. 2011a](#)). Thermal emission from the whole surface is typically not required to fit the X-ray spectrum. A notable exceptions are PSR J0437–4715 ($\nu \approx 173.7 \text{ Hz}$) and PSR J2124–3358 ($\nu \approx 202.8 \text{ Hz}$) for which combined analysis of UV and X-ray spectra allows [Durant et al. \(2012\)](#) and [Rangelov et al. \(2017\)](#) to estimate the surface temperature of these sources: $T_{\text{eff}}^\infty \sim (1 - 3) \times 10^5 \text{ K}$ and $T_{\text{eff}}^\infty \sim (0.5 - 2.1) \times 10^5 \text{ K}$, respectively. The corresponding internal temperature is $T^\infty \lesssim 10^7 \text{ K}$ and thus these pulsars are r-mode stable (even within the minimal r-mode instability model).

[Schwenzer et al. \(2017\)](#) have recently suggested a strong upper limit, $T_{\text{bb}} < 1.7 \times 10^5 \text{ K}$, on the surface tempera-

⁴ Observations of SAX J1808.4–3658 ($\nu = 401 \text{ Hz}$) can indicate that even more violent cooling is possible. The observations put an upper limit on the internal temperature $T^\infty < 1.1 \times 10^7 \text{ K}$ (e.g., [Gusakov et al. 2014a](#)), but the deep crustal heating produces $\sim 5 \times 10^{32} \text{ erg s}^{-1}$ for the average accretion rate $\dot{M} \sim 9 \times 10^{-12} M_\odot/\text{yr}$, reported by [Heinke et al. \(2009\)](#).

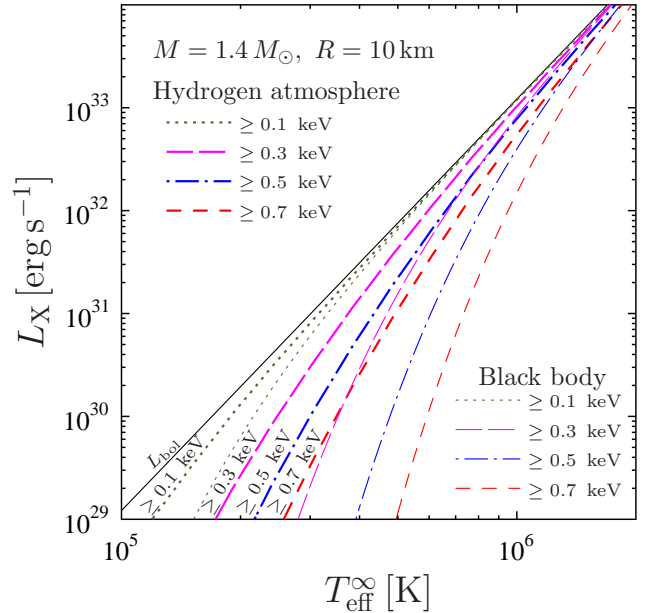


Figure 2. Thermal X-ray luminosity (as seen by a distant observer) from the whole surface of a canonical NS as a function of the effective surface temperature. Bolometric luminosity is shown by solid line, and other lines correspond to energy ranges $\geq 0.1, 0.3, 0.5,$ and 0.7 keV . Thick lines are for the hydrogen atmosphere model and thin lines – for the black-body model.

ture of PSR J1231-1411 ($\nu \approx 271.5 \text{ Hz}$) within the black-body model. As the authors emphasize, they do not account for gravitational redshift and ignore the effects related to stellar atmosphere, which can, in our opinion, significantly affect the actual value of the upper limit (see, e.g., [Zavlin, Pavlov, & Shibano 1996](#), Fig. 2 and discussion below). [Schwenzer et al. \(2017\)](#) have also proposed upper limits on the surface temperature of several other MSPs based either on estimates of their total (or, in several cases, thermal) luminosity (available in the literature) or on the results of [Prinz & Becker \(2015\)](#), who estimated maximum possible T_{bb} for a number of sources.

Here we suggest a general upper limit on the surface temperatures of MSPs. For several pulsars (e.g., for PSR 1937+21) our upper limit is stronger than that suggested by [Schwenzer et al. \(2017\)](#).

Indeed, the MSP surface temperatures are strongly constrained by existing observations: If MSPs were as hot as transiently accreting NSs, whose thermal emission is observed in X-rays even in the quiescent state (see section 2.2 and Fig. 1), the thermal emission from the whole MSP surface would be detected in X-rays as well. But it is not the case. Thus, leaving a detailed analysis of X-ray observations for each MSP beyond the scope of this paper, we assume that MSPs should (generally) be colder than the transiently accreting NSs with the measured surface temperature. To get an idea of the possible upper limit on the MSP surface temperature we rely on observations of MXB 1659–298 (assumed distance to the source $D = 10 \text{ kpc}$ and X-ray absorption column density $N_{\text{H}} = (2.0 \pm 0.2) \times 10^{21} \text{ cm}^{-2}$), IGR 00291+5934 ($D = 4 \text{ kpc}$ and $N_{\text{H}} = 2.8 \times 10^{21} \text{ cm}^{-2}$), and HETE J1900.1–2455 ($D \approx 4.7 \text{ kpc}$ and $N_{\text{H}} \approx 2.2 \times 10^{21} \text{ cm}^{-2}$), reported by [Cackett et al. \(2008\)](#), [Heinke et al.](#)

(2009), and [Degenaar et al. \(2017\)](#). For all of them the effective surface temperature was estimated as $T_{\text{eff}}^{\infty} \approx 6.3 \times 10^5$ K. Note that, for these objects both absorption column density and distances are relatively large in comparison to typical fast MSPs (with $\nu > 250$ Hz).⁵ Thus, it is unlikely that the lack of successful observations of thermal emission from the whole surface of fast MSPs can be explained by strong absorption or large distances to these sources: Rather, it is more probable that they are ‘cold’ (colder than MXB 1659–298, IGR 00291+5934, and HETE J1900.1–2455). Therefore, we choose

$$T_{\text{eff}}^{\infty} < T_{\text{eff}, \text{max}}^{\infty} = 6 \times 10^5 \text{ K} \quad (8)$$

as a fiducial upper limit for the effective surface temperature of MSPs. This temperature corresponds to the bolometric thermal luminosity $L_{\text{bol}} \lesssim 1.6 \times 10^{32} \text{ erg s}^{-1}$ [see equation (11) below]. For photon energy ranges, suitable for X-ray observations (> 0.1 , > 0.3 , and > 0.5 keV), $T_{\text{eff}}^{\infty} = 6 \times 10^5$ K corresponds to lower luminosity: $L_X^{>0.1} = 1.5 \times 10^{32}$, $L_X^{>0.3} = 1.0 \times 10^{32}$, and $L_X^{>0.5} = 0.6 \times 10^{32} \text{ erg s}^{-1}$, respectively (see also Fig. 2 which represents X-ray luminosity as a function of T_{eff}^{∞}). Here and below the upper index (e.g., >0.3) denotes the photon energy range (in keV). The quoted numbers are insensitive to the upper bound of the photon energy range (if it exceeds 1 keV) and are calculated for a canonical NS with hydrogen atmosphere (XSPEC models `nsa` by [Zavlin et al. 1996](#) and `nsatmos` by [Heinke et al. 2006](#) were applied and give the same result). The black-body model has the same bolometric luminosity (by definition of the effective temperature), but the luminosity in the X-ray part of the spectrum is much lower (compare thick and thin lines in Fig. 2 and see, e.g., [Zavlin et al. 1996](#) for details).

Polar cap and magnetospheric emission can only increase MSP luminosity, thus total unabsorbed X-ray luminosity, extracted from observations, can be applied to constrain T_{eff}^{∞} : thermal contribution can not exceed the total luminosity (in any energy range). For example, if total unabsorbed X-ray emission from some MSP is $L_X^{>0.3} < 1.0 \times 10^{32} \text{ erg s}^{-1}$, its effective temperature should be $T_{\text{eff}}^{\infty} < 6 \times 10^5$ K, confirming our constraint (8) for it. Note that, the black body emission model gives less strict constraints (see thin lines in Fig. 2; for example $L_X^{>0.3} < 1.0 \times 10^{32} \text{ erg s}^{-1}$ translates into $T_{\text{eff}}^{\infty} < 6.7 \times 10^5$ K).

Let us confront this criterion with observations. L_X was estimated for a rather large number of MSPs and, typically, $L_X^{(0.3-8)} \sim 4 \times 10^{30} - 10^{31} \text{ erg s}^{-1}$ ([Bogdanov et al. 2011b](#)), which gives $T_{\text{eff}}^{\infty} \lesssim (3.2 - 3.5) \times 10^5$ K (assuming a canonical

NS with hydrogen atmosphere), i.e. smaller than our fiducial upper limit (8). MSPs in globular cluster 47 Tuc provide yet another example suggesting that the observations put even stronger constraint on T_{eff}^{∞} than (8). This globular cluster is particularly good for X-ray studies, because it is close ($D \approx 4.5$ kpc) and weakly absorbed (cluster $N_H \approx 1.3 \times 10^{20} \text{ cm}^{-2}$, e.g., [Heinke et al. 2005](#)). [Bogdanov et al. \(2006\)](#) found X-ray counterparts for all 19 MSPs with precisely known positions in this globular cluster, and X-ray luminosity for all of them [including 47 Tuc J ($\nu \approx 476$ Hz), Y ($\nu \approx 455$ Hz), and W ($\nu \approx 425$ Hz), which were the fastest MSPs in this globular cluster known at that moment]⁶ agrees with the constraint $L_X^{(0.3-8)} \lesssim 3 \times 10^{31} \text{ erg s}^{-1}$, corresponding to $T_{\text{eff}}^{\infty} \lesssim 4.7 \times 10^5$ K. For pulsar 47 Tuc Y the flux, listed in table 3 of [Bogdanov et al. \(2006\)](#), corresponds to $L_X^{(0.3-8)} = 3 \times 10^{30} \text{ erg s}^{-1}$, setting the following upper limit on the surface temperature of this pulsar, $T_{\text{eff}}^{\infty} \lesssim 3 \times 10^5$ K. Finally, X-ray luminosity, $L_X^{0.3-8} = 10^{31} \text{ erg s}^{-1}$, reported for PSR J1810+1744 ($\nu \approx 602$ Hz) by [Gentile et al. \(2014\)](#), implies $T_{\text{eff}}^{\infty} \lesssim 3.8 \times 10^5$ K.

Some MSPs have stronger X-ray emission. For example, for PSR B1957+20 (also known as J1959+2048, $\nu \approx 622$ Hz) the unabsorbed X-ray flux in (0.15 – 10) keV range was estimated by [Arumugasamy, Pavlov, & Garmire \(2015\)](#) as $6.5 \times 10^{-14} \text{ erg cm}^{-2} \text{ s}^{-1}$, which corresponds to $L_X^{0.15-10} = 5_{-3}^{+5} \times 10^{31} \text{ erg s}^{-1}$, for $D = 2.5 \pm 1$ kpc ([Huang et al. 2012](#), inferred from the dispersion measure model of [Cordes & Lazio 2002](#)). Even the upper bound of this luminosity, $L_X^{0.15-10} = 10^{32} \text{ erg s}^{-1}$, constrains the temperature of PSR B1957+20 at $T_{\text{eff}}^{\infty} \lesssim 5.6 \times 10^5$ K, in agreement with (8).

The X-ray luminosity of MSPs with high spin-down power can be even larger. However, they have power-law X-ray spectrum and a high fraction of pulsed emission (see, e.g., section 4.2 in [Ng et al. 2014](#)). In this paper we are interested in the internal temperatures, which reveal itself in the thermal emission from the whole surface, contributing to the unpulsed component of X-ray emission. Thus, the analysis of the phase-averaged spectra can lead to overestimation of T_{eff}^{∞} . For example, for PSR B1937+21, which plays an especially important role in this paper, $L_X^{0.5-7} \approx 6.8 \times 10^{32} \text{ erg s}^{-1}$, but, as stated by [Ng et al. \(2014\)](#), it shows ‘purely non-thermal spectrum with a hard photon index of 0.9 ± 0.1 , and is nearly 100% pulsed’. Thus the thermal contribution to the unpulsed luminosity should be much smaller. Unfortunately, numerical upper bound is not reported by [Ng et al. \(2014\)](#), but violation of the constraint (8) would lead to X-ray luminosity $L_X^{(0.5-7)} > 0.6 \times 10^{32} \text{ erg s}^{-1}$, corresponding to the thermal contribution of the unpulsed fraction of X-ray emission $\gtrsim 9\%$, which exceeds an error in the determination of the unpulsed fraction of X-ray emission for B1821-24 and J0218+4232 (4% and 6%, respectively; [Ng et al. 2014](#)). Thus, we suppose that such a strong fraction of the unpulsed emission is excluded, but this conclusion should be checked by accurate analysis of the X-ray data. Note that [Schwenzer et al. \(2017\)](#) have used total X-ray luminosity ($L_X \approx 6.88 \times 10^{32} \text{ erg s}^{-1}$, quoted in their table 1) to obtain an upper limit on the surface temperature of PSR B1937+21. It can be a reason why their result

⁵ [He, Ng, & Kaspi \(2013\)](#) propose the following estimate for the absorption column density N_H : $N_H = (0.30_{-0.09}^{+0.13}) \times 10^{20} \text{ cm}^{-2}$ (DM/pc cm⁻³), where DM is the dispersion measure. Thus, MSPs with DM < 70 pc cm⁻³ should have $N_H \lesssim 2.1 \times 10^{21} \text{ cm}^{-2}$, a requirement, which is satisfied for more than 67% of currently known fast MSPs ($\nu > 250$ Hz), according to ATNF pulsar catalogue ([Manchester et al. 2005](#), catalogue version 1.55 was applied). This catalogue also gives an information on the pulsar distances, and it turns out that 70% of known fast MSPs ($\nu > 250$ Hz) are located closer than HETE J1900.1–2455, but this statistic is not independent because the pulsar distances are estimated using the [Yao et al. \(2017\)](#) DM-based distance model as default.

⁶ Recently, [Pan et al. \(2016\)](#) discovered a new pulsar in this cluster, PSR J0024-7204aa, which has a higher frequency, $\nu \approx 541$ Hz.

($T_{\text{eff}}^{\infty} \sim 10^6$ K, according to their figure 1) exceeds (8). High upper bounds for the surface temperature of some MSPs reported by [Prinz & Becker \(2015\)](#) (also quoted in table 2 in [Schwenzer et al. 2017](#)) correspond to pulsars undetected in X-rays; thus they can not be considered as evidence of violation of (8).

Summarizing, for faint X-ray pulsars [$L_X^{(0.3-8)} \lesssim 10^{31}$ erg s $^{-1}$, e.g., 47 Tuc Y $\nu \approx 455$ Hz and PSR J1810+1744 $\nu \approx 602$ Hz], total X-ray luminosity allows us to limit surface temperature at $T_{\text{eff}}^{\infty} \lesssim (3-4) \times 10^5$ K. For more luminous pulsars [$L_X^{(0.3-8)} \lesssim 10^{32}$ erg s $^{-1}$, e.g., PSR B1957+20 ($\nu \approx 622$ Hz)] T_{eff}^{∞} is constrained by our fiducial limit (8). The most luminous pulsars [$L_X^{(0.3-8)} > 10^{32}$ erg s $^{-1}$, e.g., PSR B1937+21 ($\nu \approx 642$ Hz)] typically have strong pulsed fraction, while T_{eff}^{∞} should be estimated using the unpulsed fraction of X-ray luminosity. We argue, that nearly $\sim 100\%$ pulsed emission from PSR B1937+21, reported by [Ng et al. \(2014\)](#), supports the constraint (8). An accurate and detailed analysis of X-ray and *UV* observational data can lead to even tighter upper bounds on the temperatures of MSPs. These bounds will allow one to apply the analysis of sections 3–6 in order to extract more information about the properties of these sources. However, in this paper we shall adopt the conservative general upper limit (8) and demonstrate that even it constrains the r-mode instability window.

For NSs with accreted envelope composition (a reasonable option, since they were recycled by accretion), equation (8) constrains the redshifted internal stellar temperature as

$$T^{\infty} \lesssim T_{\text{max}}^{\infty} \approx 2 \times 10^7 \text{ K} \quad (9)$$

(see the hatched region in Fig. 1). Purely iron thermally insulating envelope corresponds to a less strict constraint

$$T^{\infty} \lesssim T_{\text{max Fe}}^{\infty} \approx 4.7 \times 10^7 \text{ K}. \quad (10)$$

However, for low temperatures discussed here, an NS model with even very thin layer of accreted (light) elements strongly affects $T_{\text{eff}}^{\infty}/T^{\infty}$ ratio (see, e.g., Fig. 8 in [Potekhin et al. 1997](#)). Indeed, almost vanishing layer of light elements on top of the iron envelope with the mass $\Delta M = 4 \times 10^{-14} M_{\odot}$ reduces the estimate (10) to $T^{\infty} \lesssim 3 \times 10^7$ K, while $\Delta M \gtrsim 10^{-11} M_{\odot}$ makes it almost indistinguishable from the fully accreted result (9).⁷ Thus, we apply Eq. (9) in what follows.

Strictly speaking, equation (9) does not reveal any new inconsistency in the minimal r-mode instability model: as discussed in section 2.3, the current state of MSPs can be explained within the minimal model, assuming that they are stable, and thus even colder (see Fig. 1). However, MSP formation and intensive internal heating of PSR B1937+21 require a modification of the minimal model. As we demonstrate below, the internal temperature upper bound (9) provides an important constraint on the r-mode instability models which are able to solve the MSP formation problem (see sections 3–6).

⁷ For $T_{\text{eff}}^{\infty} \lesssim 3 \times 10^5$ K, which is a reasonable constraint for pulsar 47 Tuc Y, the internal temperature should be $T^{\infty} \lesssim 1.3 \times 10^7$ K even for iron thermally insulating envelope and $T^{\infty} \lesssim 7 \times 10^6$ K for the layer of light elements $\Delta M > 10^{-14} M_{\odot}$.

3 TINY R-MODE AMPLITUDE SCENARIO

Within the tiny r-mode amplitude scenario, NSs can be unstable, but saturation amplitudes are chosen small enough to agree with observations. [Mahmoodifar & Strohmayer \(2013\)](#) confronted this model with the observations of NSs in LMXBs and concluded that the r-mode amplitudes should range from 10^{-8} to 1.5×10^{-6} .

[Alford & Schwenzer \(2015\)](#) apply MSP timing to constrain r-mode amplitudes in MSPs.⁸ Assuming power-law dependence of relevant parameters on ν , T^{∞} , M , and R , they suggest ‘universal r-mode spin-down limit’ on gravitational wave signal from MSPs. However, at least for neutrino luminosity this assumption seems to be oversimplified: Simulations of stellar cooling and quiescent temperatures of accreting NSs require different cooling mechanisms to be active in NSs with different masses leading to very strong (non-power-law) dependence of luminosity on the mass and temperature [see, e.g., [Yakovlev & Pethick \(2004\)](#); [Page et al. \(2004\)](#); [Levenfish & Haensel \(2007\)](#); [Beznogov & Yakovlev \(2015a,b\)](#)]. Thus, universal r-mode spin-down limit suggested by [Alford & Schwenzer \(2015\)](#) should be treated with a bit of caution. Furthermore, as we demonstrate below, upper boundary (8) for the surface temperature of MSPs can constrain the r-mode amplitudes much stronger. This is in line with [Schwenzer et al. \(2017\)](#) who have recently come to the similar conclusion.

For saturated r-mode, the heating power can be estimated from equation (5). In thermal equilibrium the total heating (sum of all heating mechanisms: r-mode, rotation-induced deep crustal heating, rotochemical heating, etc.) should be compensated by cooling. If an MSP is not massive enough to open direct URCA process in its core, the neutrino emission becomes negligible [due to temperature constraint (9)], so that the total cooling luminosity can be estimated as the thermal emission from the MSP surface

$$\begin{aligned} L_{\text{cool}}^{\text{ph}} &= \frac{4\pi R^2 \sigma (T_{\text{eff}}^{\infty})^4}{1 - 2GM/(c^2 R)} \\ &\approx 1.6 \times 10^{32} \frac{\text{erg}}{\text{s}} R_{10}^2 \left(\frac{T_{\text{eff}}^{\infty}}{6 \times 10^5 \text{ K}} \right)^4, \end{aligned} \quad (11)$$

where σ is the Stefan-Boltzmann constant. Here and below the red-shift factor, $1+z = 1/\sqrt{1-2GM/(c^2 R)}$, is assumed to be 1.3. This value corresponds to the canonical NS. The upper limit on the r-mode amplitude can be computed assuming that r-modes are the only source of heat (see equation 5).⁹

$$\alpha < \alpha^{\text{ph}} = 3 \times 10^{-8} R_{10}^{-2} M_{1.4}^{-1} \nu_{500}^{-4} \left(\frac{T_{\text{eff}}^{\infty}}{6 \times 10^5 \text{ K}} \right)^2. \quad (12)$$

For massive NSs the direct URCA processes can operate in the central region of the core. Plugging the relation between

⁸ [Alford & Schwenzer \(2015\)](#) have not taken into account the correction due to Shklovskii (proper motion) effect ([Shklovskii 1970](#)), which can significantly affect $\dot{\nu}$ for some MSPs with the slowest spin-down rate (e.g., [Guillemot et al. 2016](#)).

⁹ Coefficient in equation (6) by [Schwenzer et al. \(2017\)](#) differs from ours because it corresponds to $M = M_{\odot}$, $R = 10$ km, and $L_{\text{cool}}^{\text{ph}} = 4\pi \sigma R^2 T_{\text{eff}}^4$, where $T_{\text{eff}} = (1+z)T_{\text{eff}}^{\infty}$ is the unredshifted (local) effective temperature.

the surface and internal temperatures for fully accreted envelope (Potekhin et al. 1997) into expression (7) for the neutrino luminosity, we obtain:

$$L_{\text{cool}}^{\text{URCA}} \approx 9 \times 10^{32} \frac{\text{erg}}{\text{s}} \left(\frac{T_{\text{eff}}^{\infty}}{6 \times 10^5 \text{ K}} \right)^{9.92} \left(\frac{R_{\text{D}}}{3 \text{ km}} \right)^3 \left(\frac{g_{\text{c}}}{g} \right)^{2.48}, \quad (13)$$

where

$$g = \frac{GM}{R^2 \sqrt{1 - 2GM/(c^2 R)}} \quad (14)$$

is the surface gravity (for the canonical NS $g = g_{\text{c}} = 2.43 \times 10^{14} \text{ cm/s}^2$). The luminosity (13) results in a generally weaker constraint on the r-mode amplitude,

$$\alpha < \alpha^{\text{URCA}} = 8 \times 10^{-8} \nu_{500}^{-4} R_{10}^{-0.52} M_{1.4}^{-2.24} \times \left(\frac{R_{\text{D}}}{3 \text{ km}} \right)^{1.5} \left(\frac{T_{\text{eff}}^{\infty}}{6 \times 10^5 \text{ K}} \right)^{4.96}. \quad (15)$$

If one allows for both cooling processes (photon and direct URCA), one finds the following upper limit on the r-mode amplitude,

$$\alpha < \alpha^{\text{gen}} = \sqrt{(\alpha^{\text{URCA}})^2 + (\alpha^{\text{ph}})^2}. \quad (16)$$

Note that the constraint (16) is tighter than the upper bound found by Alford & Schwenzer (2015) from the analysis of MSP spin-down rate. Thus, r-mode can be responsible only for a small fraction of the total spin down rate $\dot{\Omega}^{\text{tot}} = 2\pi\nu^{\text{tot}}$ (see Schwenzer et al. 2017 for a detailed discussion).

It is worth noting that, for $T_{\text{eff}}^{\infty} \lesssim 3 \times 10^5 \text{ K}$ [an upper limit for the surface temperature of PSR J0024–7204Y (=47Tuc Y)], the photon emission from the stellar surface dominates. Thus, in that case an upper bound on the r-mode amplitude follows *directly from observations* [by using Eq. (12)], without referencing to rather uncertain (but negligible at $T_{\text{eff}}^{\infty} \lesssim 3 \times 10^5 \text{ K}$) neutrino emission from the star.

Note also that the saturation amplitude generally increases with the temperature decrease (e.g., Bondarescu & Wasserman 2013¹⁰). Thus, an upper limit for the low-temperature MSPs is, in fact, a stronger constraint than numerically the same upper limit for hot NSs in LMXBs. In any case, the upper limit (16) on the r-mode amplitude in MSPs is too strong to be explained by previously suggested mechanisms of nonlinear saturation of r-modes (namely, saturation by nonlinear mode couplings discussed by Arras et al. 2003; Bondarescu et al. 2007; Bondarescu & Wasserman 2013 and by vortex/flux tube interaction suggested by Haskell et al. 2014). The only exception is the work by Alford, Han, & Schwenzer 2015, but it assumes a hybrid star with sharp hadron-quark interface and thus it is inapplicable to baryonic equations of state. Hence, explanation of MSPs within the tiny r-mode model is unfeasible (at least in the absence of quark core inside NSs).

At the end of the section it is worth noting that the estimates obtained above constrain the (root-mean-squared) r-mode amplitude even if it is limited not by saturation, but by the shape of the instability window (e.g., within the resonance uplift scenario; see sections 5 and 6).

¹⁰ See, however, footnote 9 in Gusakov et al. (2014a) for a critique of the low-saturation amplitude model of Bondarescu & Wasserman (2013).

4 STABILIZATION BY THE BULK VISCOSITY: TOO STRONG NEUTRINO LUMINOSITY

As discussed in section 2, shear viscosity is not sufficient to stabilize r-modes in the observed NSs. Can this problem be solved by the bulk viscosity? For nucleonic equations of state the bulk viscosity is very small at $T \lesssim 10^8 \text{ K}$, being negligible in comparison with the shear viscosity. However, for another core composition the bulk viscosity can be much larger. For example, Alford & Schwenzer (2014b) demonstrates that the model of ungapped interacting quark matter can successfully stabilize NSs in LMXBs. This model predicts that the fastest MSPs (with $\nu \gtrsim 600 \text{ Hz}$) should have internal temperatures $T \gtrsim 3 \times 10^7 \text{ K}$ (see their Fig. 1) and thus slightly contradicts the internal MSP temperature constraint (9).¹¹

Probably the more important problem of Alford & Schwenzer (2014b) is high neutrino luminosity, $L_{\text{cool}}^{\text{uiq}} \sim 4 \times 10^{37} (T_8^{\infty})^6 \text{ ergs}^{-1}$, inherent to their model.¹² For example, 4U 1608–522 is r-mode stable in ungapped interacting quark model. Thus, the main heat source for that NS is deep crustal heating. It provides $W^{\text{DCH}} \approx 2 \times 10^{34} \text{ ergs}^{-1}$ (for the average accreting rate $\dot{M} \approx 3.6 \times 10^{-10} M_{\odot}/\text{yr}$, see Heinke et al. 2007), corresponding to the equilibrium temperature $T_{\text{eq}}^{\infty} \approx 3 \times 10^7 \text{ K}$. However, this temperature is strongly below the observational estimate, $T^{\infty} \approx (0.9 - 2.5) \times 10^8 \text{ K}$ (see, e.g., Gusakov et al. 2014a). To keep 4U 1608–522 at the observed temperature there should be an additional heat source, compensating the neutrino luminosity $L_{\text{cool}}^{\text{uiq}} \approx (2 \times 10^{37} - 10^{40}) \text{ ergs}^{-1}$. The nature of such source is unclear, especially for stable NSs. The interpretation of temperatures of other hot NSs (with $T^{\infty} \sim 10^8 \text{ K}$) has the same problem.

The enhanced neutrino emission, leading to problems with explanation of hot NSs in LMXBs, should be common for models, which stabilize NSs by the bulk viscosity. The reason is simple: Both neutrino luminosity and bulk viscosity are associated with the reactions between the particles in the NS core (see, e.g., Reisenegger & Bonaćić 2003b; Gusakov, Yakovlev, & Gnedin 2005; Alford, Mahmoodifar, & Schwenzer 2010). If all these reactions are accompanied by neutrino production (as it is the case for nucleonic matter), there should be a direct correspondence between the bulk viscosity (for small-amplitude oscillations) and neutrino emissivity (see,

¹¹ According to Fig. 3 of Alford & Schwenzer (2014b), the condition (8) for T_{eff}^{∞} is fulfilled, but this figure corresponds to purely iron thermally insulating envelope, which does not look realistic in the case of MSPs (see section 2.4). For accreted envelope the ungapped interacting quark matter stability curve shifts to higher surface temperatures and violates the constraint (8).

¹² To obtain this estimate we apply equation (1) from Alford & Schwenzer (2014b), neglecting the non-Fermi-liquid effects and assuming that it is written in Plank units. Following Alford et al. (2012), we use $\Lambda_{\text{QCD}} = 1 \text{ GeV}$, $\Lambda_{\text{EW}} = 100 \text{ GeV}$. Note that these constants should not be confused with the constants denoting nonperturbative scale of QCD ($340 \pm 8 \text{ MeV}$) and scale of electroweak symmetry breaking $\approx 246 \text{ GeV}$ (e.g., Olive & Particle Data Group 2014), which often have the same notation.

for example, equations 1 and 2 in [Reisenegger & Bonačić 2003a](#), written for the modified URCA reactions). This means that enhancement of bulk viscosity unavoidably results in an enhancement of neutrino luminosity.

For more complicated core compositions (e.g., for nucleon-hyperon or quark matter) non-leptonic reactions are possible (e.g., [Jones 2001a](#); [Haensel, Levenfish, & Yakovlev 2002a](#)) that do not involve neutrinos and, being more powerful than neutrino reactions, produce dominant contribution to the bulk viscosity (e.g., [Jones 2001a](#); [Haensel, Levenfish, & Yakovlev 2002b](#); [Lindblom & Owen 2002](#); [Gusakov & Kantor 2008](#), [Alford et al. 2010](#)). Thus, the ratio of the bulk viscosity energy dissipation rate to luminosity can be enhanced in comparison to the nucleonic matter. However, to stabilize the fastest NSs in LMXBs, like 4U 1608-522, bulk viscosity should be enhanced at least by 13 orders of magnitude (cf. equations 1 and 3), which seems to be hardly possible without substantial increase in the neutrino luminosity. At the same time, if all NSs in LMXBs are r-mode stable, the quiescent temperatures of the hottest of them can be explained *only* if neutrino luminosity is not too strong, i.e., it should be on the level of the modified URCA luminosity for nucleonic cores (see, e.g., [Yakovlev & Pethick 2004](#); [Levenfish & Haensel 2007](#)).

The above arguments are, of course, not rigorous enough, but we want to stress that each particular model with r-mode stabilization by enhanced bulk viscosity should be checked for consistency with the observed quiescent temperatures of the hottest NSs in LMXBs (in particular, 4U 1608-522).

5 RESONANCE UPLIFT SCENARIO: LOW TEMPERATURE RESONANCES ARE REQUIRED

Resonance uplift scenario was suggested by [Gusakov et al. \(2014b,a\)](#) to explain observations of NSs in LMXBs. It is based on the proper account of finite temperature effects on the dynamics of superfluid liquid in the core and predicts an enhanced NS stability associated with the resonance interaction of oscillation modes in the vicinity of certain (resonance) temperatures (see Fig. 3, where the instability window is splitted by stability peaks). As discussed by [Gusakov et al. \(2014b,a\)](#), this picture agrees with detailed calculations of frequencies and damping times for: (i) r-modes and inertial modes of superfluid NSs at zero temperature ([Lee & Yoshida 2003](#); [Yoshida & Lee 2003](#)); and (ii) f- and p-modes in nonrotating superfluid NSs at finite temperatures ([Gusakov & Andersson 2006](#); [Kantor & Gusakov 2011](#); [Chugunov & Gusakov 2011](#); [Gusakov et al. 2013](#); [Gualtieri et al. 2014](#)). Furthermore, [Kantor & Gusakov \(2016\)](#) confirm the main features of the resonance uplift scenario by calculating the r-mode spectrum and damping times for a finite-temperature superfluid NS within a simplified model with vanishing entrainment. However, the form of the stability peaks depends on many parameters (e.g., on the critical temperature profiles, equation of state etc.) and remains rather uncertain. Here we shall try to constrain it by making use of the observations discussed in section 2.

As argued in [Gusakov et al. \(2014a\)](#), the fastest MSPs

should be attached to the left slopes of some of the existing stability peaks. Note that those peaks (more accurately, their left slopes) should appear at $T^\infty \lesssim T_{\text{max}}^\infty$ in order to match the observational upper limit on MSP temperature (9). Here, within the phenomenological approach, we discuss two models: (a) a model with *narrow* low-temperature stability peaks, for which the cooling luminosity L_{cool} does not change significantly inside the peak [see panel (a) in Fig. 3 and section 5.1] and (b) a model with *broad* low-temperature stability peaks [see panel (b) and section 5.2].

Formally, both models can explain the current state of the observed rapidly rotating NSs: each NS in an LMXB is either attached to the left slope of some stability peak (e.g., 4U 1608-522) or stable with respect to r-modes (e.g., XTE J1814-338), as it should be in the resonance uplift scenario (e.g., [Gusakov et al. 2014a](#)). High-frequency MSPs [with $\nu \gtrsim 450$ Hz for model (a) and $\nu \gtrsim 600$ Hz for model (b)] can be explained as moving along the left slope of the low-temperature stability peak, other MSPs should be stable. In both cases, MSP temperatures agree with observations ($T^\infty \lesssim T_{\text{max}}^\infty$). Spin frequency evolution is almost unaffected by r-modes even for high-frequency MSPs (see a discussion after equation 16). However, the recycling scenario requires that MSPs should be formed in LMXBs. In the following subsection we analyse constraints on models (a) and (b) set by this requirement.

Note that, generally, the resonance temperatures can depend not only on the microphysics input (i.e., on the equation of state, critical temperature profile, etc.), but also on the stellar mass (e.g., the appearance of hyperons in sufficiently massive NSs can change the form of the instability window dramatically). Thus, we cannot exclude the fact that both possibilities (a) and (b) are realized for different NS masses.

5.1 Narrow low-temperature stability peaks [model (a)]

Typical evolution path, which should lead to the formation of low-temperature MSPs within the model (a), is shown by a solid line in panel (a) of Fig. 3. According to the resonant uplift scenario (see [Gusakov et al. 2014a](#) for details), at the initial stage of recycling, an NS is stable and spun up by accretion; its temperature is determined by the balance between the deep crustal heating and cooling processes [$T^\infty = T_{\text{eq}}^\infty$, where T_{eq}^∞ is the solution to equation (6)]. If spin up is strong enough, NS can cross the boundary of the stability region. This leads to excitation of r-mode and accompanying heating of a star. As a result, its temperature increases. However, growth of the temperature is limited by the boundary of the stability peak, because inside the peak the star is stable and does not have a heat source to further increase T^∞ . As a consequence, subsequent NS evolution takes place along the boundary of the stability peak. The r-mode amplitude is determined by the heating power required by the thermal equilibrium condition (see [Gusakov et al. 2014a](#) for details):

$$W^r = L_{\text{cool}}(T^\infty) - W^{\text{DCH}} \quad (19)$$

To be associated with the low-temperature stability peak, located at $T^\infty = T_0^\infty$ [T_0^∞ is the ‘resonance’ temperature; see Fig. 3(a)], the equilibrium temperature should

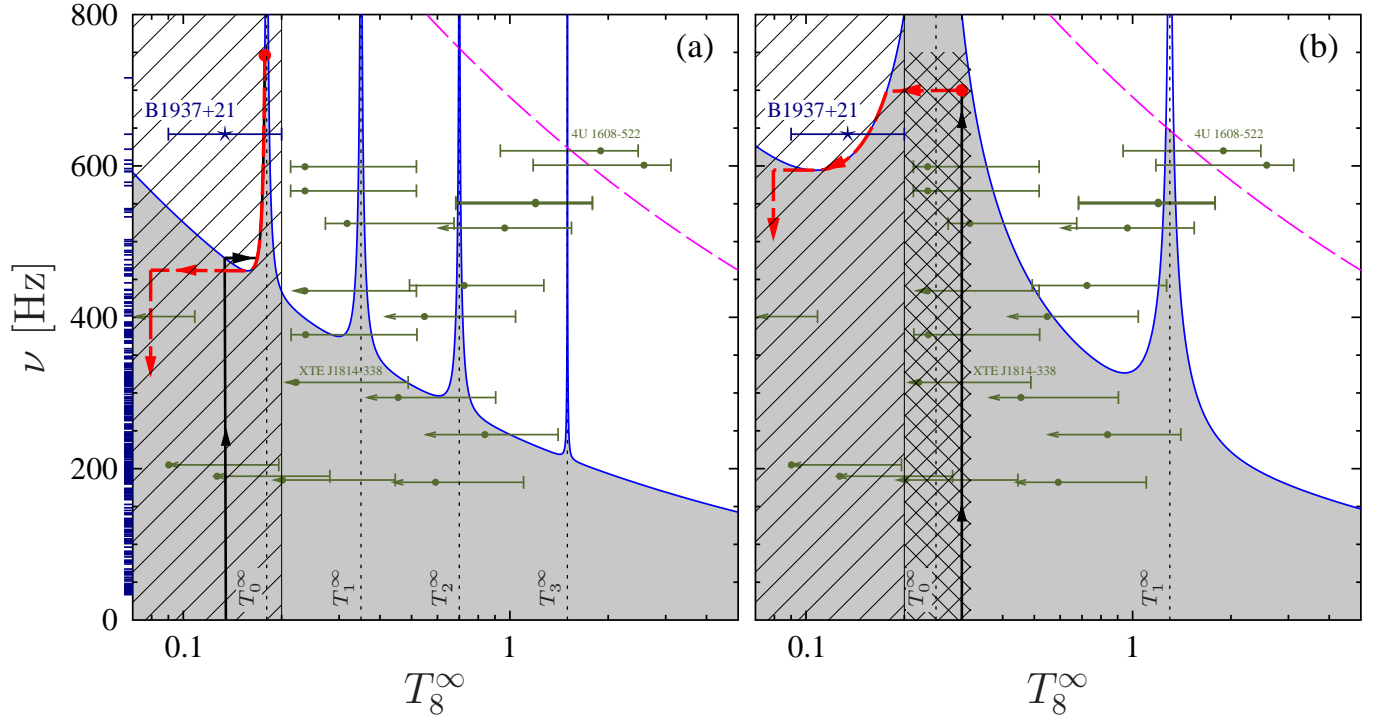


Figure 3. Example of r-mode instability windows in the resonance uplift scenario for narrow [panel (a)] and broad [panel (b)] stability peaks. The dashed line demonstrates the instability curve for $m = 3$ r-mode; all sources higher than this curve are unstable (even inside the stability peaks). Vertical dotted lines represent resonance temperatures T_i^∞ for each stability peak. Typical evolution path for an accreting NS in LMXB is shown by a thick solid line. Evolution path for a NS at the MSP stage is shown by thick dashed line. Filled circle marks the NS frequency and temperature immediately after the Roche-Lobe decoupling. Minimal stability region required for the formation of MSPs via recycling scenario is cross-hatched (see section 6 for details). Other notations are the same as in Fig. 1.

be $T_{\text{eq}}^\infty \lesssim T_0^\infty$ (in the opposite case the NS evolution in the unstable region will be associated with next stability peak at $T^\infty = T_1^\infty$). At the same time, to match the upper limit (9) on the MSP temperature, one should have $T_0^\infty < T_{\text{max}}^\infty = 2 \times 10^7$ K. In this way we obtain the first important constraint for model (a) (see equation 6):

$$\dot{M} < \dot{M}_{\text{max}} \equiv L_{\text{cool}}(T_0^\infty)/(K c^2). \quad (18)$$

The second constraint is related to accretion spin-up, which cannot increase the NS frequency above the equilibrium spin frequency $\Omega_{\text{eq}} = 2\pi\nu_{\text{eq}}$, when the net torque acting on the star is zero (for $\Omega > \Omega_{\text{eq}}$ the torque is negative). The exact numerical value of the equilibrium spin rate should be determined from the accretion theory, but it is still a subject of debate (see, e.g., Lai 2014; Parfrey, Spitkovsky, & Beloborodov 2016 and references therein). The standard model assumes that the spin equilibrium takes place when the Keplerian disc corotates with NS at the magnetosphere boundary (see, e.g., Ghosh & Lamb 1979; Wang 1995 for details)

$$\Omega_{\text{eq}} \approx \omega_c \xi^{-3/2} (GM)^{5/7} \left(\frac{\sqrt{2}\dot{M}}{\mu^2} \right)^{3/7}. \quad (19)$$

Here μ is the dipolar magnetic moment of the star; $\xi \sim 0.5 - 1.4$ and $\omega_c \lesssim 1$ are the numerical coefficients, which describe radius of the magnetosphere and spin-up efficiency.

Note that, if accreting NS is attached to the peak and accretion rate is equal to \dot{M}_{max} , the equilibrium r-mode am-

plitude (and the corresponding heating power and braking torque) are all vanish (see equation 17). Thus, at such accretion rate the r-mode instability does not affect the equilibrium frequency Ω_{eq} . For lower accretion rate, Ω_{eq} is smaller and the r-mode braking torque can only further decrease it. Thus, the maximal equilibrium frequency can be estimated as $\Omega_{\text{eq}}^{\text{max}} = \Omega_{\text{eq}}(\dot{M}_{\text{max}})$.

In real LMXBs accretion rate is evolving in time, leading to the evolution of the equilibrium spin rate (e.g., Tauris 2012). The NS spin frequency Ω cannot exceed maximum equilibrium spin frequency Ω_{eq} , which was achieved during the evolution. As far as the accretion rate cannot exceed \dot{M}_{max} at any moment of the evolution, the upper bound on the NS spin frequency in LMXB is $\Omega_{\text{eq}}^{\text{max}}$. Thus, the frequency of a newly born MSP, $\Omega_{\text{MSP}}^{\text{max}}$, also cannot exceed $\Omega_{\text{eq}}^{\text{max}}$. In fact, as it was shown by Tauris (2012), $\Omega_{\text{MSP}}^{\text{max}}$ can be even lower because MSP can lose more than a half of its rotational energy during the Roche lobe decoupling phase. Since at the MSP stage there are no accretion and any spin up torques, the stellar spin frequency can only decrease, and, as a result, it should be a subject of our second constraint,

$$\Omega < \Omega_{\text{MSP}}^{\text{max}} = p \Omega_{\text{eq}}^{\text{max}}(\dot{M}_{\text{max}}, \mu), \quad (20)$$

where the numerical parameter $p < 1$ describes spin down of MSP during the Roche lobe decoupling phase.

The third constraint comes from the requirement that the spin-down power, associated with r-modes, $\dot{E}_{\text{rot}}^r = \Omega \dot{J}_{\text{GR}}$, should not exceed the total spin-down power of

MSPs, $\dot{E}_{\text{rot}}^{\text{tot}} = I\Omega\dot{\Omega}^{\text{tot}}$. Here I is NS moment of inertia. Consider a NS evolving along the boundary of stability peak. Then the r-mode heating power is related to $\dot{E}_{\text{rot}}^{\text{r}}$ by the formula

$$W^{\text{r}} = \frac{1}{3} \left| \dot{E}_{\text{rot}}^{\text{r}} \right|, \quad (21)$$

which follows from equations (4) and (5), applied to the boundary of instability window with $\tau_{\text{eff}} = \tau_{\text{d}} = |\tau_{\text{GR}}|$. In addition, such star should be in thermal equilibrium, which means that its luminosity at the peak temperature T_0^{∞} should be equal to W^{r} , i.e., in view of equation (21),

$$L_{\text{cool}}(T_0^{\infty}) = W^{\text{r}} = \frac{\left| \dot{E}_{\text{rot}}^{\text{r}} \right|}{3} = \frac{a}{3} \left| \dot{E}_{\text{rot}}^{\text{tot}} \right| \leq \frac{1}{3} \left| \dot{E}_{\text{rot}}^{\text{tot}} \right|, \quad (22)$$

where $a = \dot{E}_{\text{rot}}^{\text{r}}/\dot{E}_{\text{rot}}^{\text{tot}} \leq 1$ is a (unknown) parameter, which determines fractional contribution of r-mode spin down at the present moment. Here we neglect other mechanisms of internal heating, which can contribute to the heating power only at a level of $\lesssim 10^{-4} \left| \dot{E}_{\text{rot}}^{\text{tot}} \right|$ (e.g., Gonzalez & Reisenegger 2010; Gusakov et al. 2015), becoming comparable to the r-mode heating only for very low values of $a \sim 3 \times 10^{-3}$.

In the remaining part of this section we put a lower limit on a following from the three constraints, discussed above, and confront this result with observations.

According to Beskin, Gurevich, & Istomin (1993); Spitkovsky (2006); Tchekhovskoy, Philippov, & Spitkovsky (2016), the spin-down power associated with magnetic field, $\dot{E}_{\text{rot}}^{\text{mag}}$, can be estimated as

$$(1 - a) \dot{E}_{\text{rot}}^{\text{tot}} = \dot{E}_{\text{rot}}^{\text{mag}} \approx -\frac{\mu^2 \Omega^4}{c^3} (1 + \sin^2 \theta). \quad (23)$$

Here θ is the magnetic dipole inclination angle and we assume that the only torques acting on an MSP are associated with r-modes and magnetic field (i.e., $\dot{E}_{\text{rot}}^{\text{tot}} = \dot{E}_{\text{rot}}^{\text{r}} + \dot{E}_{\text{rot}}^{\text{mag}}$). One can express μ from this equation and substitute it into equation (19) along with $\dot{M} = \dot{M}_{\text{max}}$ [given by equations (18) and (22)], to get $\Omega_{\text{eq}}^{\text{max}}$. The result is

$$\Omega_{\text{eq}}^{\text{max}} \approx \omega_c \xi^{-3/2} (GM)^{5/7} \left(\frac{\sqrt{2} a \Omega^4 (1 + \sin^2 \theta)}{3 K (1 - a) c^5} \right)^{3/7}. \quad (24)$$

Note that $\dot{E}_{\text{rot}}^{\text{tot}}$ is cancelled out in this final equation. It holds true for any accretion model (in particular, for the recent model of Parfrey, Spitkovsky, & Beloborodov 2016), provided that the equilibrium frequency depends on \dot{M} and μ only in combination \dot{M}/μ^2 .

Equation (24) combined with constraint (20) allows one to put a lower limit on the parameter a ,

$$a > a_{\text{min}} \approx \left[1 + 0.8(p\omega_c)^{7/3} \nu_{500}^{5/3} M_{1.4}^{5/3} (1 + \sin^2 \theta) \xi^{-7/2} \right]^{-1}. \quad (25)$$

The isolines of a_{min} are shown in Fig. 4. MSP with $M = 1.4M_{\odot}$, $\nu = 500$ Hz, and $\sin \theta = 1$ is taken as an example. Only in the most efficient spin-up scenario ($\xi \approx 0.5$, $p\omega_c \approx 1$) a_{min} can be as low as 0.05. If at least one of the parameters of the accretion model is not so optimistic, a_{min} is much larger. The larger value of a_{min} is favoured for many reasons. In particular, Tauris, Langer, & Kramer (2012) argue that $\omega_c < 1$ and $\xi > 1$ for at least some of MSPs; the

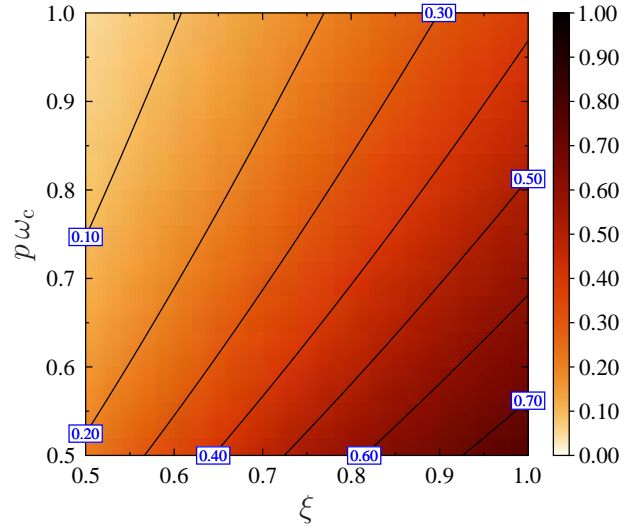


Figure 4. Example of a contour plot showing the minimum possible ratio a_{min} of the r-mode spin-down power to the total spin-down power in $(\xi, p\omega_c)$ plane. To plot the figure we choose $\nu = 500$ Hz, $\sin \theta = 1$, and $M = 1.4M_{\odot}$.

most efficient model ($p = 1$) does not account for spin-down both during the Roche lobe decoupling phase (Tauris 2012) and at the MSP stage; recent model by Parfrey et al. (2016) suggests that ω_c should be very small for small ξ ; finally, smaller angle θ leads to higher a_{min} . Furthermore, to obtain an upper limit for the spin frequency (20) we assume accretion rate to be equal to its upper limit, $\dot{M} = \dot{M}_{\text{max}}$. If real \dot{M} is lower, the equilibrium spin frequency is lower too, leading to a stronger lower bound on a . All in all, we believe that a realistic value of a_{min} should exceed 0.05.

Let us confront the constraint (25) with observations. Unfortunately, direct detection of gravitational wave signal from r-modes is impossible, because (at least, for high frequency MSPs, $\nu \geq 300$) it is below the sensitivity level of advanced LIGO due to very small r-mode amplitudes allowed in MSPs (see section 3 and, e.g., Alford & Schwenzer 2015). Another almost straightforward procedure to measure a is associated with the so called α -oscillations – modulations of r-mode amplitude, which are unavoidable for MSPs evolving along a narrow stability peak (Kantor et al. 2016). This modulation leads to ‘anti-glitches’ – sudden drops of MSP frequency on a time-scale of hours-months. Such features have not been found yet in MSP timing, thus observations can be used to put an upper limit on a . Indeed, in the limiting case $a \approx 1$, almost all MSP spin-down should be associated with ‘anti-glitch’ events, which clearly contradicts observations. At the same time, our preliminary results indicate that $a = 0.05$ can agree with timing residuals for PSR B1937+21, reported in Reardon et al. (2016). We leave the problem of accurate determination of an upper limit for a to subsequent studies.

Constraint (25) can also be checked indirectly. According to equation (21), r-mode contribution to the spin down unavoidably leads to NS heating. Thus, equation (25) determines the minimum heating power for MSP evolving along a narrow low-temperature stability peak,

$$W_{\text{min}}^{\text{r}} = \frac{a_{\text{min}}}{3} \left| \dot{E}_{\text{rot}}^{\text{tot}} \right|. \quad (26)$$

This heating can be too strong to be balanced by cooling at low temperature. For example, taking the moment of inertia $I = 10^{45} \text{ g cm}^2$, PSR B1937+21 has $|\dot{E}_{\text{rot}}^{\text{tot}}| \sim 10^{36} \text{ erg s}^{-1}$. Thus, for the lowest possible value of $a_{\text{min}} = 0.05$, the minimal r-mode heating power is $W_{\text{min}}^r \sim 2 \times 10^{34} \text{ erg s}^{-1}$. Even assuming that fully unsuppressed hyperon URCA is open in the central region with the radius $R_{\text{D}} = 3 \text{ km}$, this heating power is sufficient to heat the star up to a temperature $T^\infty \approx 3 \times 10^7 \text{ K}$ [see equation (7)], which exceeds the upper limit (9) by a factor of 1.5. As noted above, if accretion spin-up is not extremely efficient, a_{min} should be much larger, substantially complicating the explanation of MSPs with $|\dot{E}_{\text{rot}}^{\text{tot}}| \gtrsim 10^{35} \text{ erg s}^{-1}$. Thus, the model with narrow low-temperature resonance peaks should be rejected (at least) for pulsars with high spin-down power. But what about the model (b) with broad low-temperature stability peaks?

5.2 Broad low-temperature stability peaks [model (b)]

Typical evolution path in case of broad low-temperature peaks [model (b)] is shown in panel (b) of Fig. 3. During the LMXB stage an NS evolves inside the stability peak. Its temperature is determined by the deep crustal heating (see equation 6) and the spin frequency is controlled by accretion. After Roche-lobe decoupling [filled circle in panel (b) of Fig. 3] accretion stops, and the NS becomes an MSP, which cools down by photon and neutrino emission. If its frequency is high enough [$\gtrsim 594 \text{ Hz}$ for the example shown in Fig. 3(b)], cooling stops at the left boundary of the stability peak and the r-mode excites up to an amplitude required to keep NS in thermal equilibrium [see equation (17) with $W^{\text{DCH}} = 0$]. In the opposite case, MSP stays stable (r-mode is not excited) and evolves to the left until the thermal equilibrium with other (less effective) heating processes (see section 2.3) is established.

In order to explain observations of MSPs model (b) should satisfy two main requirements:

(A) Temperature of the left slope of the low-temperature stability peak should not exceed the observational constraint (9) in the whole MSP frequency range.

(B) Accretion should be able to spin the star up to high frequencies *within* the low-temperature peak [in the opposite case, immediately after an NS reaches the high-temperature boundary of the peak, the r-modes will be excited, heating the star up to the next (high-temperature) stability peak, so that the subsequent evolution will be associated with that peak].

The constraint (25) is unjustified in case of broad low-temperature resonances because the cooling luminosity decreases significantly during cooling of a newly born MSP inside the stability peak. As a result, the contribution of r-modes to the spin down of MSPs can be very small.

Both requirements (A) and (B) can be satisfied by adjusting the parameters of the low-temperature stability peak. For example, in Fig. 3(b) the requirement (A) holds true up to $\nu < 800 \text{ Hz}$. The requirement (B) can be satisfied by adjusting the high-temperature slope of stability peak, as it was done in Fig. 3(b). Indeed, the fact that a num-

ber of high-frequency accreting NSs (which are progenitors of MSPs according to the recycling scenario) are contained inside the broad stability peak shown in 3(b) can serve as an indirect evidence that the requirement (B) is fulfilled for this model.

We can also check the consistency of a broad-peak model with requirement (B) for certain accretion model. For example, the standard accretion model predicts the following minimum accretion rate, required to spin up an (r-mode stable) MSP with the observed ν and $\dot{\nu}$,

$$\dot{M}_{\text{min}} = \frac{c^3 \xi^{7/2}}{2^{1/2} G^{5/3} p^{7/3} \omega_c^{7/3} (1 + \sin^2 \theta)} \frac{I \dot{\Omega}}{M^{5/3} \Omega^{2/3}} \quad (27)$$

[see, e.g., Tauris et al. 2012; the same result can also be derived from equations (19), (20), and (23)]. This accretion rate corresponds to the minimal power of deep crustal heating,

$$W_{\text{min}}^{\text{DCH}} = c^2 K \dot{M}_{\text{min}} \approx 3.6 \times 10^{33} \text{ erg s}^{-1} \frac{\dot{\nu}_{14} I_{45}}{\nu_{500}^{2/3} M_{1.4}^{5/3}} \quad (28)$$

where in the last equality we assume $\xi = 0.5$, $p = \omega_c = \sin(\theta) = 1$, $K = 10^{-3}$, $\dot{\nu}_{14} = \dot{\nu}/10^{-14} \text{ Hz s}^{-1}$, and $I_{45} = I/10^{45} \text{ g cm}^2$. For a (stable) NS inside the stability peak this heating should be compensated by cooling, providing a constraint on the *minimal* NS temperature at the LMXB stage, $T^\infty \gtrsim T_{\text{eq, min}}^\infty$, where $T_{\text{eq, min}}^\infty$ is found from

$$L_{\text{cool}}(T_{\text{eq, min}}^\infty) = W_{\text{min}}^{\text{DCH}}. \quad (29)$$

For example, the strongest (among the known MSPs) $W_{\text{min}}^{\text{DCH}} \approx 1.4 \times 10^{34} \text{ erg s}^{-1}$ corresponds to PSR B1937+21 (assuming $I_{45} = 1$). It can be compensated by unsuppressed hyperon direct URCA (assuming $R_{\text{D}} = 3 \text{ km}$) at $T_{\text{eq, min}}^\infty \approx 3.1 \times 10^7 \text{ K}$. Thus, the temperature of this NS at LMXB stage should not be less than this value. At $T^\infty = 3.1 \times 10^7 \text{ K}$ the high frequency boundary of the broad stability peak in Fig. 3(b) corresponds to $\nu \approx 750 \text{ Hz}$, thus PSR B1937+21 (with $\nu \approx 642 \text{ Hz}$) could, in principle, be spun up by accretion on the LMXB stage, without leaving out this stability peak.

To explain NSs observed in LMXBs with higher temperatures, our model (b) requires also high-temperature stability peaks. As it is argued in Chugunov et al. (2014), NSs associated with such peaks evolve not to MSPs, but to so called ‘HOFNARs’. These NSs maintain high temperature due to r-mode instability even after the end of accretion epoch in LMXBs and should be observed in X-rays because of their high surface temperatures, $T_{\text{eff}}^\infty \sim 10^6 \text{ K}$. Some of the candidates to quiescent LMXB systems (qLMXBs) – X-ray sources, whose spectra are interpreted as thermal emission from the whole NS surface, but accretion episodes have never been detected (see, e.g., Guillot et al. 2011) – can, in fact, belong to that new class. As discussed in Chugunov et al. (2014) HOFNARs can have very low magnetic fields due to Ohmic dissipation and thus do not reveal themselves as radio pulsars. Non-detection (to our best knowledge) of radio emission from qLMXB candidates (=HOFNARs candidates) supports this statement. The lower bound on the r-mode contribution to the spin-down (equation 25) can also be applied to HOFNARs, but it is not restricting, because their spin-down can, in fact, be generated purely by r-modes.

α -oscillations can be suppressed for NS evolving along

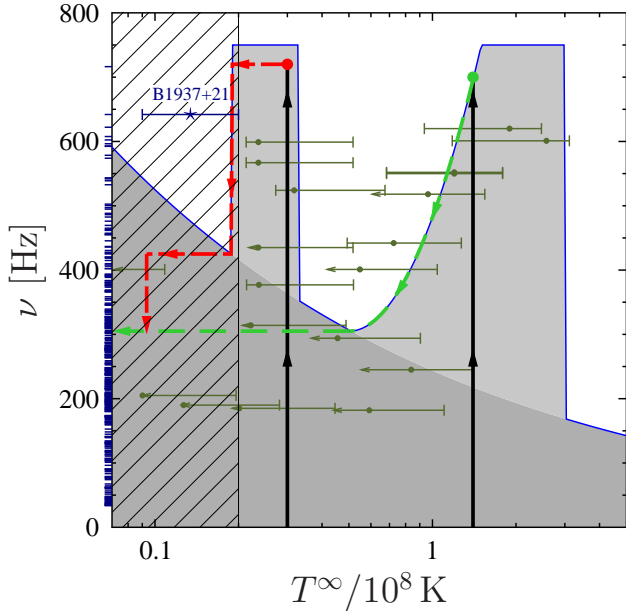


Figure 5. An example of a minimally constrained r-mode instability window. The evolution tracks, leading to the formation of MSPs and HORNARs are shown by thick lines with arrows (solid lines correspond to evolution at the LMXB stage, dashed lines — after it). Regions of enhanced stability (in comparison to the minimal model of section 2.1) are shown by lighter shading. Other notations are the same, as in Fig. 1.

the broad stability peaks (Kantor et al. 2016). Thus, absence of ‘anti-glitches’ would not allow one to draw any conclusion about validity of the model with broad stability peak. However, if anti-glitches were observed, it would provide strong constraints on the parameters of the stability peaks.

6 GENERAL CONSTRAINTS ON THE R-MODE INSTABILITY WINDOW

The constraints on the resonance uplift scenario obtained in section 5 appeal only to the shape of the instability window, but not to the actual physics which determines that shape. Thus, our results are equally applicable to arbitrary r-mode instability model with similar morphology of the stability region (a set of humps of enhanced stability located at certain temperatures, see Fig. 5).¹³ They can be formulated as follows (an example of the instability window, satisfying the constraints below, is shown in Fig. 5) :

(I) To explain formation of MSPs in agreement with the upper limit (9) on MSP temperature, the r-mode instability should be suppressed in the whole MSP frequency range ($\nu \lesssim 750$ Hz) at least for temperatures $T_{\max}^{\infty} \lesssim T^{\infty} \lesssim T_{\text{eq, min}}^{\infty}$ [cross-hatched region in Fig. 3(b)]. Here $T_{\text{eq, min}}^{\infty}$ is given by equation (29). $T_{\text{eq, min}}^{\infty}$ is specific for each MSP, but the strongest bound (the largest $T_{\text{eq, min}}^{\infty}$) comes from PSR

¹³ More complicated stability windows, e.g., like those suggested in Gusakov et al. (2014a) (see Appendix D there), cannot also be excluded.

B1937+21. In case of the standard accretion model and the direct URCA emissivity (see equation 7) it corresponds to $T_{\text{eq, min}}^{\infty} \sim 3.1 \times 10^7$ K (assuming $R_D = 3$ km) and becomes higher if cooling and/or accretion spin up is less efficient.

(II) The r-mode instability can be unsuppressed at low temperatures ($T^{\infty} < T_{\max}^{\infty}$) and, if it is the case, it can, in principle, be confirmed by observations. Namely, if minimum of the instability curve for $T^{\infty} < T_{\max}^{\infty}$ takes place at a point ($T_{\min}^{\infty}, \nu_{\min}$) (e.g., in Fig. 3(b) $T_{\min}^{\infty} \approx 10^7$ K and $\nu_{\min} \approx 594$ Hz), all MSPs with $\nu > \nu_{\min}$ should have $T^{\infty} > T_{\min}^{\infty}$ and can be affected by anti-glitches, associated with α -oscillations (if they are not suppressed).

(III) Strictly speaking, current observations do not require to stabilize all NSs observed in LMXBs by one hump – the r-mode instability can be almost unsuppressed in the region 7×10^7 K $\lesssim T^{\infty} \lesssim 10^8$ K [as in Figs. 3(b) and 5]. However, at larger temperatures instability should be suppressed by additional hump (may be narrow) to explain the hottest NSs in LMXBs with $T^{\infty} \sim 10^8$ K (e.g., 4U 1608-522). Such stars should evolve not to MSPs, but to HOFNARs, as suggested by Chugunov et al. (2014) (see high temperature stability hump in Fig. 5 and correspondent evolution track).

At the end let us note that the constraint (I) can be used to quickly check various r-mode instability models for consistency with fiducial MSP temperature upper bound (9), which assumes accreted thermally insulating envelope (see section 2.4 for details). For example, some of the models discussed in the recent review by Haskell (2015) disagree with this constraint. Namely, the model with strong mutual friction and ‘strong’ superfluidity (left panel of Fig. 3 in that paper) predicts that all MSPs with $\nu \gtrsim 550$ Hz should have internal temperature $T \gtrsim 3 \times 10^7$ K. It can agree with (8) only for the layer of accreted material $\Delta M \lesssim 10^{-12} M_{\odot}$ (assuming a canonical NS). The strange star model (Fig. 4 of Haskell 2015) predicts even larger temperatures, requiring lower ΔM .

7 CONCLUSIONS

We put new constraints on the shape of the r-mode instability window. They follow from the recycling scenario and observations of (a) NSs in LMXBs (section 2.2), (b) MSP timing (section 2.3) and (c) UV and X-ray observations of MSPs (section 2.4). Analysing the observational sets (a) and (b), which have already been used to put an upper bound on the r-mode instability by several authors, we emphasize the importance of two points: (i) any successful model should not only suppress the instability for NSs observed in LMXBs, but also explain their temperatures (this is especially important for models based on an enhanced bulk viscosity, see section 4); (ii) internal heating mechanisms [superfluid vortex creep (Alpar et al. 1984), rotochemical heating (Reisenegger 1995), and rotation-induced deep crustal heating (Gusakov, Kantor, & Reisenegger 2015)] are strong enough to make PSR B1937+21 unstable within the minimal r-mode instability model, providing thus new evidence of additional dissipation of r-modes at low temperatures. One more constraint comes from the observational set (c), which allows us to put an upper limit on the internal MSP temperature, $T^{\infty} \lesssim T_{\max}^{\infty} \approx 2 \times 10^7$ K, limiting thus the maximum possible r-mode amplitude in MSPs (section 3).

These results qualitatively agree with similar conclusions of [Schwenzer et al. \(2017\)](#). Combined with the recycling scenario of MSP formation, the temperature upper limit (9) allows us to conclude that the r-mode instability should be suppressed in the whole MSP frequency range ($\nu \lesssim 750$ Hz) at temperatures $2 \times 10^7 \text{ K} \lesssim T^\infty \lesssim 3 \times 10^7 \text{ K}$ (see Fig. 5 and section 6 for details). This condition can be used to quickly check for consistency various instability windows available in the literature. In particular, it can be fulfilled in the resonance uplift scenario suggested by [Gusakov et al. \(2014b,a\)](#) (see section 5 for a detailed analysis).

It is worth noting, that constraining the surface temperature of the fastest MSPs by detailed analysis of X-ray and *UV* observational data can be a very interesting task. It is very likely that such analysis can put much more stringent upper limits on the surface temperatures of individual sources, than our general upper limit $T_{\text{eff}}^\infty \lesssim 6 \times 10^5 \text{ K}$ (see section 2.4, and [Schwenzer et al. 2017](#)). This can make the r-mode instability even more tightly constrained. In the opposite case, if one observes an MSP with higher temperature, it will be even more important, because it will present an almost direct evidence of r-mode instability in such pulsar: The thermal emission from the surface $L_{\text{cool}}^{\text{ph}} \gtrsim 10^{32} \text{ erg s}^{-1}$ should have an energy source, and the r-mode instability seems to be the most natural ‘energy supplier’ in the absence of accretion.¹⁴

ACKNOWLEDGEMENTS

We are very grateful to Dima Zyuzin for suggesting us the paper by [He et al. \(2013\)](#) and to an anonymous referee for useful comments. This study was supported by the Russian Science Foundation (Grant No. 14-12-00316).

REFERENCES

Alford M. G., Han S., Schwenzer K., 2015, *Phys. Rev. C*, 91, 055804
 Alford M. G., Mahmoodifar S., Schwenzer K., 2010, *Journal of Physics G Nuclear Physics*, 37, 125202
 Alford M. G., Mahmoodifar S., Schwenzer K., 2012, *Phys. Rev. D*, 85, 024007
 Alford M. G., Schwenzer K., 2014a, *ApJ*, 781, 26
 Alford M. G., Schwenzer K., 2014b, *Physical Review Letters*, 113, 251102
 Alford M. G., Schwenzer K., 2015, *MNRAS*, 446, 3631
 Alpar M. A., Cheng A. F., Ruderman M. A., Shaham J., 1982, *Nature*, 300, 728
 Alpar M. A., Pines D., Anderson P. W., Shaham J., 1984, *ApJ*, 276, 325
 Andersson N., 1998, *ApJ*, 502, 708
 Andersson N., Kokkotas K., Schutz B. F., 1999a, *ApJ*, 510, 846
 Andersson N., Kokkotas K. D., Stergioulas N., 1999b, *ApJ*, 516, 307
 Andersson N., Jones D. I., Kokkotas K. D., 2002, *MNRAS*, 337, 1224

¹⁴ Other internal heating mechanisms have efficiency $W^i \lesssim 10^{-4} \left| \dot{E}_{\text{rot}}^{\text{tot}} \right|$ (see [Gonzalez & Reisenegger 2010](#); [Gusakov et al. 2015](#)), producing $W^i \lesssim 10^{32} \text{ erg s}^{-1}$ even for MSPs with the highest spin down power, $\left| \dot{E}_{\text{rot}}^{\text{tot}} \right| \sim 10^{36} \text{ erg s}^{-1}$.

Arras P., Flanagan E. E., Morsink S. M., Schenk A. K., Teukolsky S. A., Wasserman I., 2003, *ApJ*, 591, 1129
 Arumugasamy P., Pavlov G. G., Garmire G. P., 2015, *ApJ*, 814, 90
 Beskin V. S., Gurevich A. V., Istomin Y. N., 1993, *Physics of the pulsar magnetosphere*. Cambridge University Press
 Beznogov M. V., Yakovlev D. G., 2015a, *MNRAS*, 447, 1598
 Beznogov M. V., Yakovlev D. G., 2015b, *MNRAS*, 452, 540
 Bildsten L., 1998, *ApJ*, 501, L89
 Bisnovatyi-Kogan G. S., Komberg B. V., 1976, *Sov. Astron. Lett.*, 2, 130
 Bogdanov S., Archibald A. M., Hessels J. W. T., Kaspi V. M., Lorimer D., McLaughlin M. A., Ransom S. M., Stairs I. H., 2011a, *ApJ*, 742, 97
 Bogdanov S., Grindlay J. E., Heinke C. O., Camilo F., Freire P. C. C., Becker W., 2006, *ApJ*, 646, 1104
 Bogdanov S. et al., 2011b, *ApJ*, 730, 81
 Bondarescu R., Teukolsky S. A., Wasserman I., 2007, *Phys. Rev. D*, 76, 064019
 Bondarescu R., Wasserman I., 2013, *ApJ*, 778, 9
 Brown E. F., Bildsten L., Rutledge R. E., 1998, *ApJ*, 504, L95
 Cackett E. M., Wijnands R., Miller J. M., Brown E. F., Degenaar N., 2008, *ApJ*, 687, L87
 Chandrasekhar S., 1970, *Phys. Rev. Lett.*, 24, 611
 Chen H.-L., Chen X., Tauris T. M., Han Z., 2013, *ApJ*, 775, 27
 Chugunov A. I., Gusakov M. E., 2011, *MNRAS*, 418, L54
 Chugunov A. I., Gusakov M. E., Kantor E. M., 2014, *MNRAS*, 445, 385
 Cordes, J. M., & Lazio, T. J. W. 2002, *ArXiv e-prints* (arXiv:astro-ph/0207156)
 Degenaar N., Ootes L. S., Reynolds M.T., Wijnands R., Page D., 2017, *MNRAS*, 465, L10
 Durant M., Kargaltsev O., Pavlov G. G., Kowalski P. M., Posselt B., van Kerkwijk M. H., Kaplan D. L., 2012, *ApJ*, 746, 6
 Friedman J. L., Lindblom L., Lockitch K. H., 2016, *Phys. Rev. D*, 93, 024023
 Friedman J. L., Morsink S. M., 1998, *ApJ*, 502, 714
 Friedman J. L., Schutz B. F., 1978a, *ApJ*, 221, 937
 Friedman J. L., Schutz B. F., 1978b, *ApJ*, 222, 281
 Gentile P. A. et al., 2014, *ApJ*, 783, 69
 Ghosh P., Lamb F. K., 1979, *ApJ*, 234, 296
 Glampedakis K., Andersson N., 2006a, *Phys. Rev. D*, 74, 044040
 Glampedakis K., Andersson N., 2006b, *MNRAS*, 371, 1311
 Gonzalez D., Reisenegger A., 2010, *A&A*, 522, A16
 Gualtieri L., Kantor E. M., Gusakov M. E., Chugunov A. I., 2014, *Phys. Rev. D*, 90, 024010
 Guillemot L. et al., 2016, *A&A*, 587, A109
 Guillot S., Rutledge R. E., Brown E. F., Pavlov G. G., Zavlin V. E., 2011, *ApJ*, 738, 129
 Gusakov M. E., Andersson N., 2006, *MNRAS*, 372, 1776
 Gusakov M. E., Chugunov A. I., Kantor E. M., 2014a, *Phys. Rev. D*, 90, 063001
 Gusakov M. E., Chugunov A. I., Kantor E. M., 2014b, *Phys. Rev. Lett.*, 112, 151101
 Gusakov M. E., Kantor E. M., 2008, *Phys. Rev. D*, 78, 083006
 Gusakov M. E., Kantor E. M., Chugunov A. I., Gualtieri L., 2013, *MNRAS*, 428, 1518
 Gusakov M. E., Kantor E. M., Reisenegger A., 2015, *MNRAS*, 453, L36
 Gusakov M. E., Yakovlev D. G., Gnedin O. Y., 2005, *MNRAS*, 361, 1415
 Haensel P., Levenfish K. P., Yakovlev D. G., 2002a, *A&A*, 394, 213
 Haensel P., Levenfish K. P., Yakovlev D. G., 2002b, *A&A*, 381, 1080
 Haskell B., 2015, *International Journal of Modern Physics E*, 24, 1541007

- Haskell B., Andersson N., Passamonti A., 2009, MNRAS, 397, 1464
- Haskell B., Degenaar N., Ho W. C. G., 2012, MNRAS, 424, 93
- Haskell B., Glampedakis K., Andersson N., 2014, MNRAS, 441, 1662
- He C., Ng C.-Y., Kaspi V. M., 2013, ApJ, 768, 64
- Heinke C. O., Grindlay J. E., Edmonds P. D., Cohn H. N., Lugger P. M., Camilo F., Bogdanov S., Freire P. C., 2005, ApJ, 625, 796
- Heinke C. O., Jonker P. G., Wijnands R., Deloye C. J., Taam R. E., 2009, ApJ, 691, 1035
- Heinke C. O., Jonker P. G., Wijnands R., Taam R. E., 2007, ApJ, 660, 1424
- Heinke C. O., Rybicki G. B., Narayan R., Grindlay J. E., 2006, ApJ, 644, 1090
- Ho W. C. G., Andersson N., Haskell B., 2011, Phys. Rev. Lett., 107, 101101
- Ho W. C. G., Lai D., 2000, ApJ, 543, 386
- Huang R. H. H., Kong A. K. H., Takata J., Hui C. Y., Lin L. C. C., Cheng K. S., 2012, ApJ, 760, 92
- Jones P. B., 2001a, Phys. Rev. D, 64, 084003
- Jones P. B., 2001b, Physical Review Letters, 86, 1384
- Kantor E. M., Gusakov M. E., 2011, Phys. Rev. D, 83, 103008
- Kantor E. M., Gusakov M. E., 2016, presentation at “New-CompStar meeting on oscillations and instabilities in neutron stars”, Southampton, UK, 13 - 14 September 2016. <http://www.southampton.ac.uk/stag/news/events/2016/09/13-newcompstar-meeting-oscillations-and-instabilities-in-neutron-stars.pdf> (accessed October 20, 2016)
- Kantor E. M., Gusakov M. E., Chugunov A. I., 2016, MNRAS, 455, 739
- Lai D., 2014, in European Physical Journal Web of Conferences, Vol. 64, European Physical Journal Web of Conferences, p. 01001
- Lee U., Yoshida S., 2003, ApJ, 586, 403
- Levenfish K. P., Haensel P., 2007, Astrophys. Space Sci., 308, 457
- Levin Y., 1999, ApJ, 517, 328
- Levin Y., Ushomirsky G., 2001, MNRAS, 324, 917
- Lindblom L., Mendell G., Owen B. J., 1999, Phys. Rev. D, 60, 064006
- Lindblom L., Owen B. J., 2002, Phys. Rev. D, 65, 063006
- Lindblom L., Owen B. J., Morsink S. M., 1998, Phys. Rev. Lett., 80, 4843
- Mahmoodifar S., Strohmayer T., 2013, ApJ, 773, 140
- Manchester R. N., Hobbs G. B., Teoh A., Hobbs M., 2005, AJ, 129, 1993
- Nayyar M., Owen B. J., 2006, Phys. Rev. D, 73, 084001
- Ng C.-Y., Takata J., Leung G. C. K., Cheng K. S., Philippopoulos P., 2014, ApJ, 787, 167
- Oertel M., Hempel M., Klähn T., Typel S., 2016, Rev. Mod. Phys. (accepted) ArXiv e-prints (arxiv:1610.03361)
- Olive K., Particle Data Group, 2014, Chinese Physics C, 38, 090001
- Owen B. J., 2010, Phys. Rev. D, 82, 104002
- Özel F., Freire P., 2016, ARA&A, 54, 401
- Page D., Lattimer J. M., Prakash M., Steiner A. W., 2004, ApJS, 155, 623
- Pan Z., Hobbs G., Li D., Ridolfi A., Wang P., Freire P., 2016, MNRAS, 459, L26
- Parfrey K., Spitkovsky A., Beloborodov A. M., 2016, ApJ, 822, 33
- Potekhin A. Y., Chabrier G., Yakovlev D. G., 1997, A&A, 323, 415
- Prinz T., Becker W., 2015, ArXiv e-prints (arxiv:1511.07713)
- Rangelov B., Pavlov G. G., Kargaltsev, O., Reisenegger A., Guillot S., van Kerkwijk M., Reyes C., 2017, ApJ, 835, 264
- Reardon D. J. et al., 2016, MNRAS, 455, 1751
- Reisenegger A., 1995, ApJ, 442, 749
- Reisenegger A., Bonačić A., 2003a, in Pulsars, AXPs and SGRs Observed with BeppoSAX and Other Observatories, Cusumano G., Massaro E., Mineo T., eds., pp. 231–236
- Reisenegger A., Bonačić A., 2003b, Phys. Rev. Lett., 91, 201103
- Rieutord M., 2001, ApJ, 550, 443
- Schwenzer K., Boztepe T., Güver T., Vurgun E., 2017, MNRAS, 466, 2560
- Shklovskii I. S., 1970, Soviet Ast., 13, 562
- Shternin P. S., Yakovlev D. G., 2008, Phys. Rev. D, 78, 063006
- Spitkovsky A., 2006, ApJ, 648, L51
- Tauris T. M., 2012, Science, 335, 561
- Tauris T. M., Langer N., Kramer M., 2012, MNRAS, 425, 1601
- Tchekhovskoy A., Philippov A., Spitkovsky A., 2016, MNRAS, 457, 3384
- Wang Y.-M., 1995, ApJ, 449, L153
- Watts A. L., Krishnan B., Bildsten L., Schutz B. F., 2008, MNRAS, 389, 839
- Yao J. M., Manchester R. N., Wang N., 2017, ApJ, 835, 29
- Yakovlev D. G., Kaminker A. D., Gnedin O. Y., Haensel P., 2001, Phys. Rep., 354, 1
- Yakovlev D. G., Pethick C. J., 2004, ARA&A, 42, 169
- Yoshida S., Lee U., 2003, MNRAS, 344, 207
- Zavlin V. E., 2007, Ap&SS, 308, 297
- Zavlin V. E., Pavlov G. G., Shibano Y. A., 1996, A&A, 315, 141
- Zdunik J. L., Fortin M., Haensel P., 2017, A&A, 599 A119